UNIVERSITY OF OKLAHOMA

GRADUATE COLLEGE

INVESTIGATION OF THE MECHANICAL AND MICROSTRUCTURAL PROPERTIES IN CORONARY ARTERIES FOLLOWING DECELLULARIZATION

SUBMITTED TO THE GRADUATE FACULTY

in partial fulfillment of the requirements for the

Degree of

MASTER OF SCIENCE

By

ELIZABETH ANNE BRADSHAW

Norman, Oklahoma

2023

INVESTIGATION OF THE MECHANICAL AND MICROSTRUCTURAL PROPERTIES IN CORONARY ARTERIES FOLLOWING DECELLULARIZATION

A THESIS APPROVED FOR THE
STEPHENSON SCHOOL OF BIOMEDICAL ENGINEERING

BY THE COMMITTEE CONSISTING OF

Dr. Chung-Hao Lee, Chair

Dr. Rebecca Scott

Dr. Stefan Wilhelm

This thesis is dedicated to my family, friends, and fiancé.

Table of Contents

List of Figures

List of Tables

Acknowledgements

First, I would like to acknowledge and thank my advisor, Dr. Chung-Hao Lee for all the guidance and support he has given me over the last three years. When I first joined his lab, I had no idea what direction I wanted my career to go, but despite the obstacles presented by COVID-19, Dr. Lee has helped me discover my passion for research. I would also like to thank my committee, Dr. Rebecca Scott, and Dr. Stefan Wilhelm for their consideration of my thesis. Dr. Scott and Dr. Wilhelm have been critical in my development as a student and as a researcher.

Next, I would like to thank my fellow researchers in the Biomechanics and Biomaterials Design Laboratory for their support, guidance, and friendship. Importantly, I would like to express my gratitude to Colton, Sergio, Devin, Katie, and many more. Finally, I would like to thank my parents, my brother, my fiancé, my friends, and my pets. Without their love and support, none of this would have been possible.

Abstract

The heart is responsible for pumping blood throughout the body, and like all other tissues, the heart muscle requires a supply of oxygen-rich blood to function properly. This blood is supplied by the coronary arteries – the network of blood vessels on the surface of the heart. There are two main coronary arteries: the left (main) coronary artery and the right coronary artery. The left coronary artery divides into the left anterior descending artery (LADA) and the left circumflex artery. The LADA is the largest of the coronary arteries, and it is the most susceptible to disease. Coronary artery disease is characterized by plaque accumulation on the inner arterial wall, which limits the blood flow to the heart muscle and can result in a heart attack. In severe coronary artery disease, surgeons perform a procedure called coronary artery bypass grafting (CABG), which bypasses the diseased portion of the artery by using a graft to redirect blood from the aorta to the portion of the artery distal from the blockage. Usually, this graft comes from another artery within the patient's body; however, this is not always ideal due to limited availability of viable vessels and high graft failure rates. When autologous grafts are unable to be used, a vessel conduit is required, however, current coronary artery conduits are suboptimal. An alternative approach to tissue-engineered vascular grafts is utilizing a donor vessel's native extracellular matrix (ECM) to serve as a scaffold. To minimize the risk of an immune response from the patient, the donor vessel oftentimes needs to be decellularized to remove all cellular components. While decellularization remains a promising approach, there is not a standardized decellularization method for coronary arteries, and there is a lack of research investigating how the microstructure behaves under pathologic loads following decellularization. This thesis addresses this gap by proposing a novel protocol for the decellularization of porcine coronary artery tissue that effectively removes cellular components, while retaining the native

tissue structure and function. This decellularization protocol consists of several treatments using detergents, enzymes, and rinsing steps, and the removal of cells is confirmed using histology and microscopic evaluation. To further determine the effect of this decellularization procedure on the mechanical properties and collagen fiber architecture, biaxial mechanical testing and polarized spatial frequency domain imaging (pSFDI) were performed before and after decellularization. This investigation revealed minimal alteration to the mechanical and microstructural properties. The findings of this thesis will be valuable to the refinement of coronary artery tissue grafts, which may ultimately improve suboptimal outcomes in coronary bypass surgeries.

CHAPTER 1 – INTRODUCTION

1.1 Motivation

The heart requires a constant supply of oxygen to function properly. This oxygen is delivered to the heart muscle through a system of blood vessels, called coronary arteries. In the case of coronary artery disease (CAD), the buildup of plaque along the inner arterial wall narrows the lumen and reduces the amount of blood flow through the artery. If left untreated, CAD can result in the complete occlusion of the artery, which can lead to a heart attack. When CAD is severe or multiple vessels are occluded, other vessels in the patient's body are used as grafts to surgically bypass the blocked region of the coronary artery. However, autologous grafts can be limited in quality and quantity, and they have a relatively high rate of failure. When autologous grafts are unable to be used, a vessel conduit is required, however, current coronary artery conduits are sub-optimal. Commercially available synthetic tissue-engineered vascular grafts (TEVG) for coronary artery bypass have demonstrated poor long-term performance. An alternative approach to tissue engineered vascular grafts is utilizing a donor vessel's native extracellular matrix (ECM) to serve as a scaffold. In order to minimize the risk of an immune response from the patient, the donor vessel is decellularized to remove all cellular components. While decellularization remains a promising approach, there is not a standardized decellularization method for coronary arteries, and there is a lack of research investigating how the microstructure behaves under pathological loads following decellularization. Therefore, there is a critical need to characterize the coronary artery microstructure composition, collagen fiber architecture, and biaxial mechanical properties before and after decellularization.

1.2 Objective and Scope

The objective of this thesis is to first develop a decellularization procedure for the LADA, and to analyze the effect of the chosen decellularization treatment on the microstructural and biaxial mechanical characteristics of the porcine left anterior descending artery. The studies performed to achieve this goal are as follows:

1. Decellularization optimization of the left anterior descending artery and the characterization of artery microstructure using histology.

   In this study, a left anterior descending artery was sectioned into nine strips and exposed to a solution of Triton X-100 and a second solution of DNase and RNase. The tissue strips were exposed to the solutions for 0, 12, and 24 hours. Hematoxylin and eosin stains were used to verify decellularization.

2. Biaxial Mechanical characterization and collagen microstructural analysis pre- and post-decellularization treatment.

   In this study, twelve left anterior descending arteries were biaxially tested under pathological loading conditions before and after treatment, either with the detergent, enzyme, and rinse solutions for the test group, or just the rinse solutions for the control group. The tissues were placed under various forces in the circumferential and longitudinal directions to stimulate *in vivo* conditions. Polarized spatial frequency domain imaging (pSFDI) was used to determine collagen alignment under these loading conditions.

The remainder of this thesis is organized as follows. Chapter 2 of this thesis provides relevant background information, including the anatomy and function of the coronary arteries, artery pathology and current treatment options. An overview of the advancements and gaps in tissue-

engineered vascular grafts is also provided. Chapter 3 describes the methods and results of the optimized decellularization protocol on the left anterior descending artery, and Chapter 4 presents the methods and results of the biaxial characterization and pSFDI tests. Finally, Chapter 5 concludes this thesis with discussion of the key findings and future areas of investigation based upon this research.

CHAPTER 2 – LITERATURE REVIEW

2.1 Coronary Artery Anatomy and Function

2.1.1 Coronary Artery Vascular System

The coronary arteries are a network of blood vessels on the surface of the heart that supply the oxygenated blood to the myocardium. As illustrated in **Figure 2-1**, the coronary vascular system consists of two primary arteries: the right coronary artery (RCA) and the left main coronary artery (LMCA). The RCA directs blood flow from the anterior ascending aorta to the right atrium and ventricle, and it further branches off into the right posterior descending artery and the marginal artery. On the other hand, the LMCA is divided into the left anterior descending artery (LADA) and the left circumflex artery (LCA). The LADA supplies blood to the anterior side of the left ventricle while the LCA supplies blood to the left atrium and the lateral wall of the left ventricle[1].

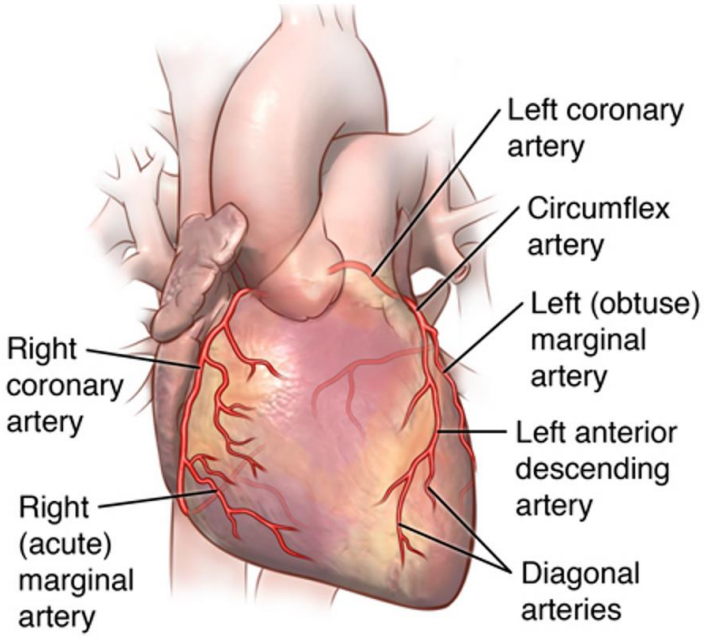

Figure 2-1: Schematic of the Coronary Artery Anatomy. Adapted from hopkinsmedicine.com

2.1.2 Coronary Artery Morphology

The coronary arterial walls consist of three primary layers: the tunica adventitia, media, and intima, as shown in **Figure 2-2**. The adventitia is the outermost layer of the artery, and it is primarily composed of collagen fibers, elastin fibers, fibroblasts, and glycoproteins such as proteoglycans and glycosaminoglycans (GAGs). This layer protects the vessel from over stretching and connects the vessel to surrounding tissues[2]. The collagen and elastin in the inner adventitia form layered structures with varied orientations, while the outer regions of the adventitia had collagen fibers that were more randomly arranged. When no load is applied, the collagen fibers appear wavy and the elastin fibers are straight. The primary orientation of the elastin fibers was found to be parallel to the collagen fiber orientation, although secondary orientations were present[3].

Between the tunica adventitia and the tunic media is a thin layer of elastin called the external elastic membrane. This elastic membrane provides structural support and the ability to stretch. The tunica media is the thickest layer of the coronary arteries, and it is predominately made up of smooth muscle cells and elastin fibers. This layer allows for vasoconstriction and relaxation of the vessel. At the boundary between the tunica media and intima lies the internal elastic membrane. Similar to the external elastic membrane, the internal elastic membrane provides support and stretching capabilities. The tunica intima comprises of epithelial cells and connective tissue. The intima is lined with a simple layer of squamous endothelial cells called the endothelium[4]. Extending from the endothelium into the lumen is the endothelial glycocalyx, which is a network of proteoglycans and glycoproteins[5]. Adjacent to the endothelium is the basement membrane, which connects the epithelial cells to the connective tissue. The basement membrane is predominately composed of laminins and type IV collagen. The outermost layer of

the tunica intima is made up of elastin and collagen fibers[4].

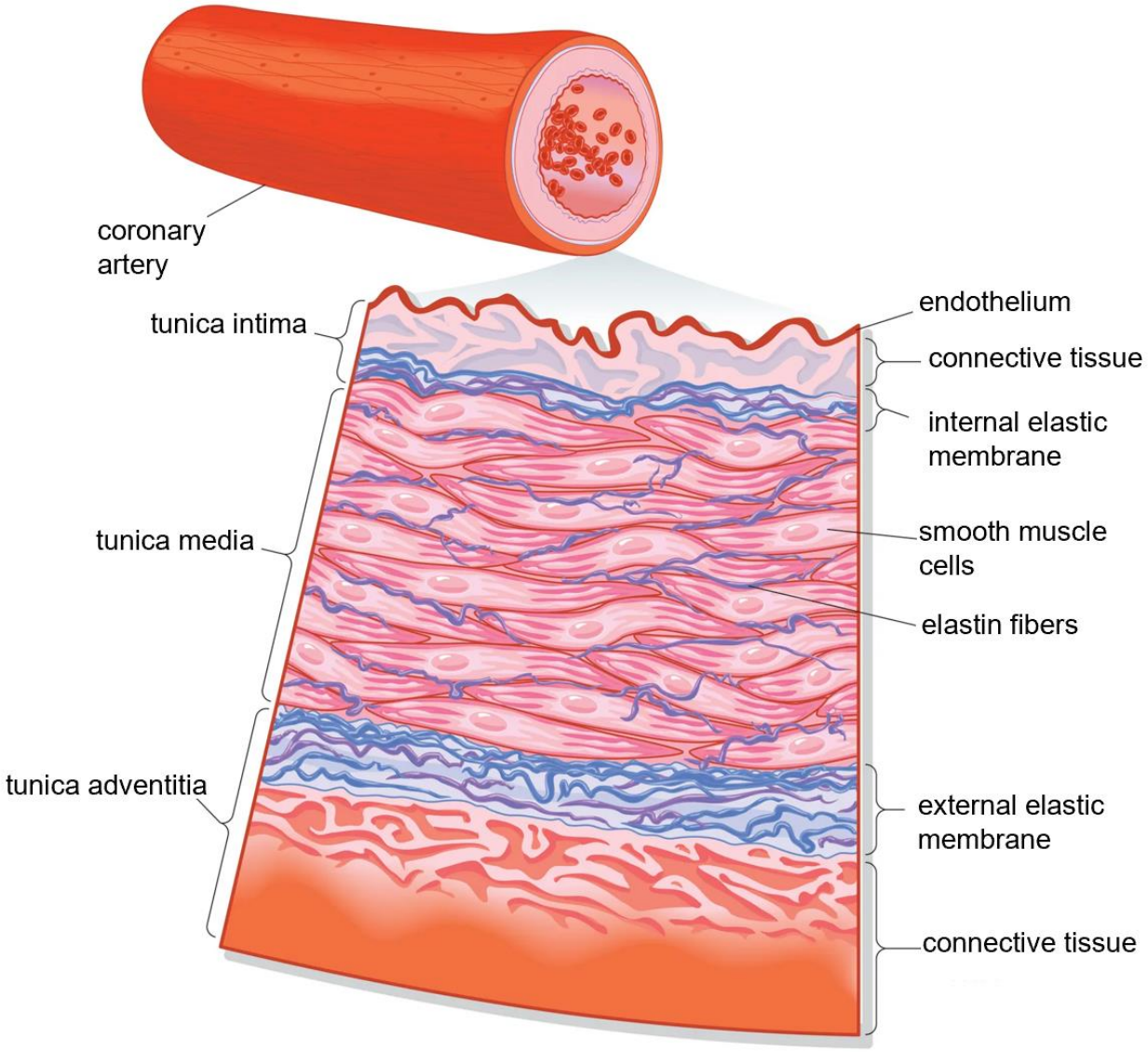

Figure 2-2: Coronary Artery Microstructure. Adapted from 2010 Encyclopedia Britannica.

2.1.3 Coronary Artery Mechanical Properties

The mechanical properties of arteries are closely related to the underlying microstructure. The primary longitudinal orientation of the collagen and elastin in the adventitia layer produces a larger longitudinal stress, while the tunica media induces a higher circumferential stress attributed by the circumferential orientation of the smooth muscle cells and elastin fibers[2]. In

arteries, the elastin fibers are less stiff than the collagen fibers, and they can deform more. Elastin is responsible for elastic recoil, and allows the arteries to repeatedly undergo stress and relaxation cycles[6]. Because collagen forms sublayers with uniform alignment, the deformation of arterial collagen is more homogeneous than the deformation of arterial elastin, that is more variably dispersed and oriented[3]. In 2022, Pineda-Castillo *et al*. analyzed the mechanical properties of the regions of the LADA, and found that the LADA displayed anisotropic nonlinear stress-stretch responses when exposed to biaxial tensions[7].

2.2 Coronary Artery Disease and Current Treatment Options

2.2.1 Description

Coronary artery disease (CAD) is the leading cause of death in the United States, and it accounts of approximately 610,000 deaths annually[8]. CAD is caused by atherosclerosis, which is the accumulation of plaque along the inner artery walls. These deposits of plaque are composed of fatty compounds, cholesterol, calcium, fibrin, and cellular waste. It is hypothesized that the occurrence of cholesterol-containing lipoproteins binding to intimal proteoglycans is a key process in the development of atherosclerosis. These low-density lipoproteins become oxidized and induce a cascade of inflammatory responses that leads to the formation of macrophage foam cells. The accumulation of foam cells results in the progression of vessel fatty streaks, which eventually progresses into plaque[6]. This plaque narrows the arterial lumen, which restricts the flow of blood to the heart muscle, potentially leading to myocardial infarction (MI), left ventricular dysfunction (LVD), and heart failure (HF)[9]. This gradual buildup of plaque is depicted in **Figure 2-3**.

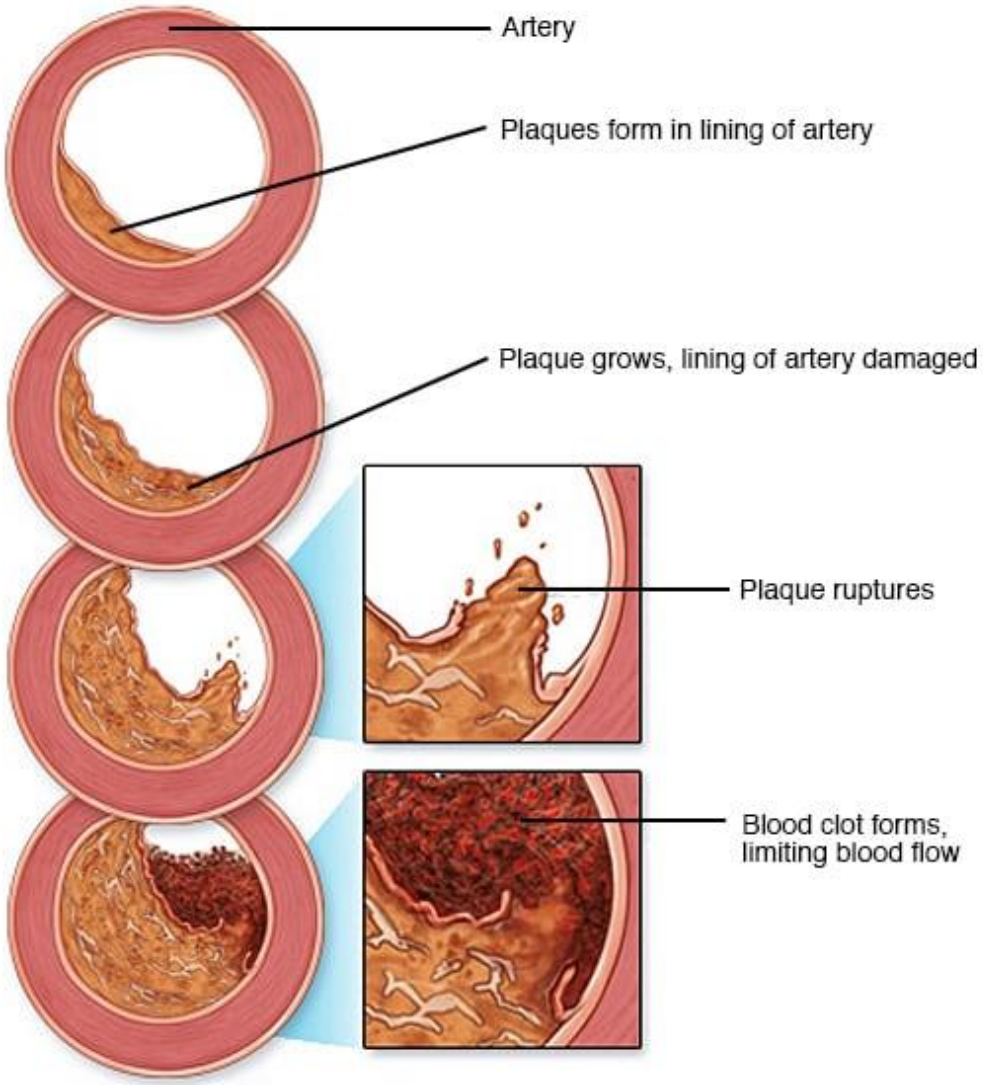

Figure 2-3: Progression of Coronary Artery Disease. Adapted from Mayo Clinic.

The LADA is the arterial region that is most susceptible to disease. It is hypothesized that the hemodynamic compression of the bifurcated septal branches and low shear stress lead to a higher risk of plaque formation[10].

2.2.2 Current Clinical Treatment Options

CAD can be managed through modification of diet and lifestyle to reduce the risk of disease progression, or it can be treated more aggressively through pharmaceutical or surgical intervention. Pharmaceutical therapies include antiplatelet and anticoagulant agents, angiotensin-converting enzyme (ACE) inhibitors, β-blockers, statins, calcium channel blockers, and nitrates[9].

There are currently two main methods of surgical treatment of CAD: (i) balloon angioplasty combined with stenting and (ii) coronary artery bypass grafting (CABG)[9]. An angioplasty, also known as percutaneous coronary intervention (PCI), is a minimally invasive procedure in which a small balloon is attached to the tip of a catheter that is guided through a blood vessel to the blocked artery. The balloon is temporarily inflated, pushing the plaque towards the arterial walls and allowing more lumen space for blood flow. Next, a small mesh stent is introduced and expanded to permanently fill the newly opened space. The two commonly used types of stents are bare metal stents and drug-eluting stents[11].

In cases where there are multiple occluded vessels, patients have improved survival outcomes and fewer revascularization surgeries when treated using CABG compared to PCI[12]. CABG is a surgical procedure that bypasses the diseased portion of the artery by using a graft to redirect blood from the aorta to the portion of the artery distal from the blockage. Usually, grafts used in these surgeries come from other arteries or veins within the patient's body, with the most common conduits being the internal thoracic arteries (ITA), radial arteries (RA) and great saphenous veins (GSV)[13].

While the strategy of CABG improves patient outcomes for those with advanced coronary artery disease and multi-vessel occlusions, the use of autologous grafts has many limitations. One such limitation is that a substantial proportion of grafts fail[14]. Saphenous veins,

for instance, have a failure rate of around 50% in 5 to 10 years after CABG surgery[15]. RAs have a failure rate at 10 years of 9-11%, and ITAs have a failure rate of 5-15%.[14] While the ITA and RA have better long-term patency, the harvesting and preparation of these vessels is technically more demanding, and there are greater risks involved[16–18]. It is hypothesized that one reason why autologous grafts fail is the mismatch in conduit morphology and mechanical properties. In 2016, Prim *et al*. characterized the mechanical and structural differences between porcine LADA, ITA, RA, and GSV[19]. They found that the elastin distribution and fractional percentage differs between the LADA and the other conduits. The GSV and RA contain fewer medial elastin fibers, and the ITA has a much higher percentage of elastin than the LADA. Similarly, the collagen and smooth muscle cell proportions also differed between the LADA and the conduits. The RA and GSV both had a significantly lower collagen fraction and a larger smooth muscle cell fraction than the LADA. In addition, the grafts were mechanically tested under the approximated loading conditions for the coronary environment and compared to the *in-situ* conditions. Prim *et al*. found that the RA and GSV had significantly higher inner radii and a circumferential stress in the coronary environment compared to their *in-situ* state. This mismatch could contribute to these grafts having a higher rate of failure when compared to the ITA, that has an environment more closely matched to the coronary artery[19]. Besides graft failure, autologous grafts are also limited in availability and quality, which can be a limitation in the treatment of multi-vessel CAD or when vascularization surgeries need to be redone after graft failure[20,21].

2.2.3 Tissue-Engineered Grafts

Due to the limitations of autologous grafts for revascularization procedures, there is a critical need for tissue-engineered vascular grafts (TEVG). These TEVGs can be made from natural biological materials, synthetic materials, or a combination of natural and synthetic materials. Synthetic vessels have demonstrated sufficient long-term results when substituting for vessels with a large diameter (>9mm) and medium diameter (6-8mm); however, synthetic small-diameter (<6mm) vessels have shown poorer patency[17]. Challenges in vascular tissue engineering include mimicking mechanical properties of the native tissue, immunogenic response, and thrombogenicity[22,23].

An alternative to synthetic grafts is the use of decellularization of allografts or xenografts to create vessel scaffolds. In order to use grafts that originate from human or animal cadavers, it is necessary to remove the cellular components of the tissue to avoid triggering an adverse immune response[24]. Decellularization is a technique to remove native cells and the genetic material from biological tissue to create a natural scaffold from the extracellular matrix (ECM). With the microstructure and mechanical properties of the ECM intact, the scaffold can then be *recellularized* with autologous cells to create a functional graft. Different strategies to achieve decellularization include physical methods, chemical and enzymatic methods, and a combination of the two[25].

Physical treatments rely on physical mechanisms to lyse cells . These methods include thermal shock, hydrostatic pressure, and supercritical fluids. The freeze-thaw method uses thermal shock to rupture cell membranes. This cycle involves alternating the temperature of the tissue from -80 °C to 37 °C, which is the average *in vivo* human body temperature. Although this method retains the tissue's biochemical properties, it has been found to be associated with

damage to the ECM[24]. Another physical treatment method is to use hydrostatic pressure, where tissue is exposed to high pressures over 600 MPa to disturb the cells inside the tissue. In a study using hydrostatic pressure to decellularize porcine vessels, it was found that this method was successful in destroying cells, but *the cellular debris remained on the scaffold*[26]. A less common physical method of decellularization uses supercritical fluids, which are the liquid forms of substances like carbon dioxide, that have surpassed their critical points in temperature and pressure. This technique has demonstrated satisfactory decellularization without compromising tissue's mechanical or structural properties. However, the expensive and complicated system needed to generate these supercritical fluids has limited its general application[24].

Decellularization can also be achieved using chemical and enzymatic treatments. The most common chemical method of decellularization is the use of surfactants. Surfactants work by rupturing the phospholipid bilayer. This occurs because the surfactants contain both hydrophobic and hydrophilic ends, that can break up the cell membrane. Of the surfactants, there are three main categories: ionic, non-ionic, and zwitterionic. In the ionic detergents, the polar heads of the molecules are either positively or negatively charged. The non-ionic detergents have non-polar heads, and the zwitterionic detergents contain both negatively and positively charged heads. The most commonly used ionic detergents for decellularization are sodium dodecyl sulfate (SDS) and sodium deoxycholate (SD). Triton X-100 and 3-[(3-cholamidopropyl)dimethylammonio]-1-propanesulfonate (CHAPS) are the most commonly used non-ionic and zwitterionic detergents, respecitvely[25]. SDS is efficient in its removal of cellular materials, however, it has been found to denature structural proteins and alter mechanical properties. Additionally, SDS is cytotoxic, so it must be thoroughly washed from the scaffold prior to recellularization. The ionic detergent, SD, is less toxic than SDS, but it is limited in its ability to fully decellularize the tissue because it

causes aggregation of DNA molecules on the surface of the scaffold. In contrast to ionic surfactants, non-ionic surfactants, like Triton X-100, are non-toxic and preserve the ECM structure and mechanical properties. These detergents work by targeting lipid-lipid interactions in the cell membrane to create pores. However, some studies have found that Triton X-100 can result in remnant cellular material[25,27]. The zwitterionic detergent, CHAPS, has demonstrated good preservation of ECM and lysis of cells, but some studies have found residual cytoplasmic proteins on the scaffold[24].

Another chemical decellularization method involves the use of acids and bases. Some acid and base methods utilize peracetic acid and alkaline reversible swelling. However, the use of peracetic acid is associated with incomplete cell removal as well as protein denaturation. The technique of reversible swelling works by the alkaline solution inducing a negative charge on the tissue's collagen. This swelling is then reversed when treated with ammonium sulfate. When paired with a non-ionic detergent, the alkaline swelling technique has been shown to effectively remove cells while maintaining ECM structural properties. However, the use of alkaline solution showed a reduction of GAGs and elasticity that was not seen using the detergent alone[25].

Enzymes are commonly used along with other methods to help facilitate the process of decellularization. DNase is used commonly in combination with Triton X-100 and SD to further break down DNA remnants that could cause immunogenicity. Other enzymes that are used include RNase, endonuclease, and Trypsin. Trypsin, which works by breaking down cell-matrix adhesive, is commonly used in combination with ethylenediaminetetraacetic acid (EDTA). When the tissue is exposed to this combination for a short period of time, the ECM remains intact, but the removal of cells is incomplete[28]. However, when exposed longer to completely remove DNA traces, this protocol can lead to a reduction in GAGs, collagen, and elastin. Due to the

inefficiency of this combination alone, it is typically only used briefly prior to further treatment with other methods[25].

While there are many different decellularization strategies, there is no universal standard for effectively decellularizing coronary arteries. Moreover, current coronary artery decellularization studies do not systematically evaluate the change in microstructure and mechanical properties of the vessels as a result of the decellularization procedure[29]. Therefore, there is a critical need to generate an effective decellularization procedure for vessel grafts that does not damage the ECM or mechanical properties.

2.4 Purpose of study

The overall objective of this thesis is thus to provide a novel decellularization method for porcine coronary arteries and to demonstrate how this decellularization procedure impacts the microstructural and mechanical properties of the artery. Previous studies of this nature have either not shown complete decellularization, or the microstructure and mechanical properties were not examined, or they were altered. We hypothesize that the proposed decellularization protocol using Triton X-100 and RNase and DNase will effectively remove cellular content from the porcine coronary arteries without altering the microstructure and mechanical properties of the arteries.

CHAPTER 3 – DECELLULARIZATION

A decellularization procedure was optimized to determine the minimum treatment exposure time that sufficiently removes cellular and genetic materials. Reducing the treatment exposure time minimizes the potential damage to the ECM and its mechanical properties. The success of decellularization was determined using hematoxylin and eosin (H&E) stains and visualized using light microscopy.

3.1 Method

To determine the optimal decellularization procedure, the LADA was isolated from three porcine hearts acquired from a local slaughterhouse (Chickasha Meat Company, Chickasha, OK, USA.) The LADA isolation process is shown in **Figure 3-1**. Following dissection, tissue samples were stored in a freezer at -20 °C until the time of the decellularization experiment.

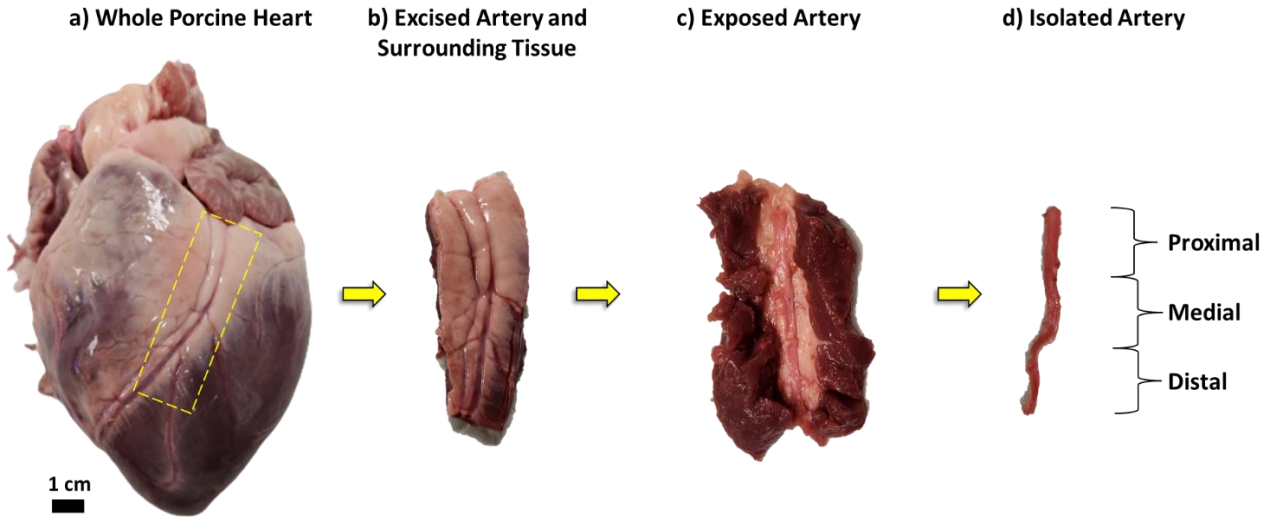

Figure 3-1: Photographs showing the dissection process for the LADA: a) The whole porcine heart and the dashed lines indicating where the artery and surrounding tissue were cut; b) The excised artery and surrounding tissue; c) The exposed artery from making a series of longitudinal cuts in the myocardium; d) The isolated artery divided into three subparts: proximal, medial, and distal.

A matrix of nine testing conditions were used to determine the optimal exposure times for decellularization using Triton X-100 and an enzymatic solution of DNase and RNase. A 500 mL solution of 0.5% Triton X-100 was made from mixing 2.5 mL Triton X-100 (Sigma-Aldrich) and 497.5 mL deionized (DI) water. An enzymic solution of 0.02 mg/mL of RNase and 0.2 mg/mL of DNase was made by adding 2 mg of RNase (Sigma-Aldrich) and 20 mg of DNase (Sigma-Aldrich) to 100 mL phosphate-buffered saline (PBS) with 50 mMol $MgCl_2$ (Sigma-Aldrich).d The tissue samples were exposed to a combination of these solutions with exposure times ranging from 0 to 24 hours with an interval of 12 hours that was first determined in an internal pilot study (results not shown here). The exposure times are summarized in **Table 3-1**.

Table 3-1: Detergent and enzyme exposure times (hours) for each tissue sample

Test No.	Detergent Exposure Time (hours)	Enzyme Exposure Time (hours)
1	0	0
2	0	12
3	0	24
4	12	0
5	12	12
6	12	24
7	24	0
8	24	12
9	24	24

Using the proximal and medial regions of the LADA, nine thin strips of roughly equal size were cut from the artery. Each tissue sample was then placed in a 1.5 mL micro-vial of the first solution (0.5% Triton X-100 + DI water) for the specified amount of time at room temperature. Following exposure to the first solution, each tissue sample was washed in DI water for 24 hours in another 1.5 mL micro-vial at room temperature. After being rinsed in DI water, the tissue samples were placed into the second solution (0.2 mg/mL DNase + 0.02 mg/mL RNase + PBS) for the specified amount of time. Following exposure to the second solution, the tissue samples were washed in a solution of PBS for 24 hours. Immediately after the PBS wash, the tissue samples were next placed in tissue cassettes and in a solution of 10% formalin (Sigma-Aldrich) for 48 hours and then subsequently stored in 20% ethanol. The tissue samples in the solutions are shown in **Figure 3-2**. This experiment was repeated for a sample size of n=3.

Figure 3-2: Artery tissue segments in Triton X-100 or DI water.

To qualitatively examine the success of the decellularization procedure, the tissue samples were evaluated via standard histopathology. First, the tissue samples were incrementally dehydrated with alcohol, cleared with xylene, and then infiltrated with paraffin. Following paraffin infiltration, the tissue samples were embedded into wax blocks and cut into 5-micron slices. The slices were placed in a 40 °C water bath and positioned on charged microscope slides. Following this, the slides were stained with hematoxylin and eosin (H&E), and the results were viewed using a light microscope. Hematoxylin stains the cell nuclei purple, while eosin stains the extracellular matrix pink. This histology procedure is explained in more detail in **Appendix – C**.

To examine the effect of the decellularization procedure on the artery microstructural components, the arteries were stained with Masson's trichrome and elastic van Gieson (EVG).

Masson's trichrome stains collagen blue, cell nuclei black/dark purple, and muscle and cytoplasm red/purple. EVG stains elastin black/dark purple, collagen red, and muscle yellow.

3.2 Results

The resulting images from the H&E-stained tissues were compared to determine which procedure most sufficiently removed cellular components. **Figure 3-3** shows the images taken using a light microscope with a 40X objective.

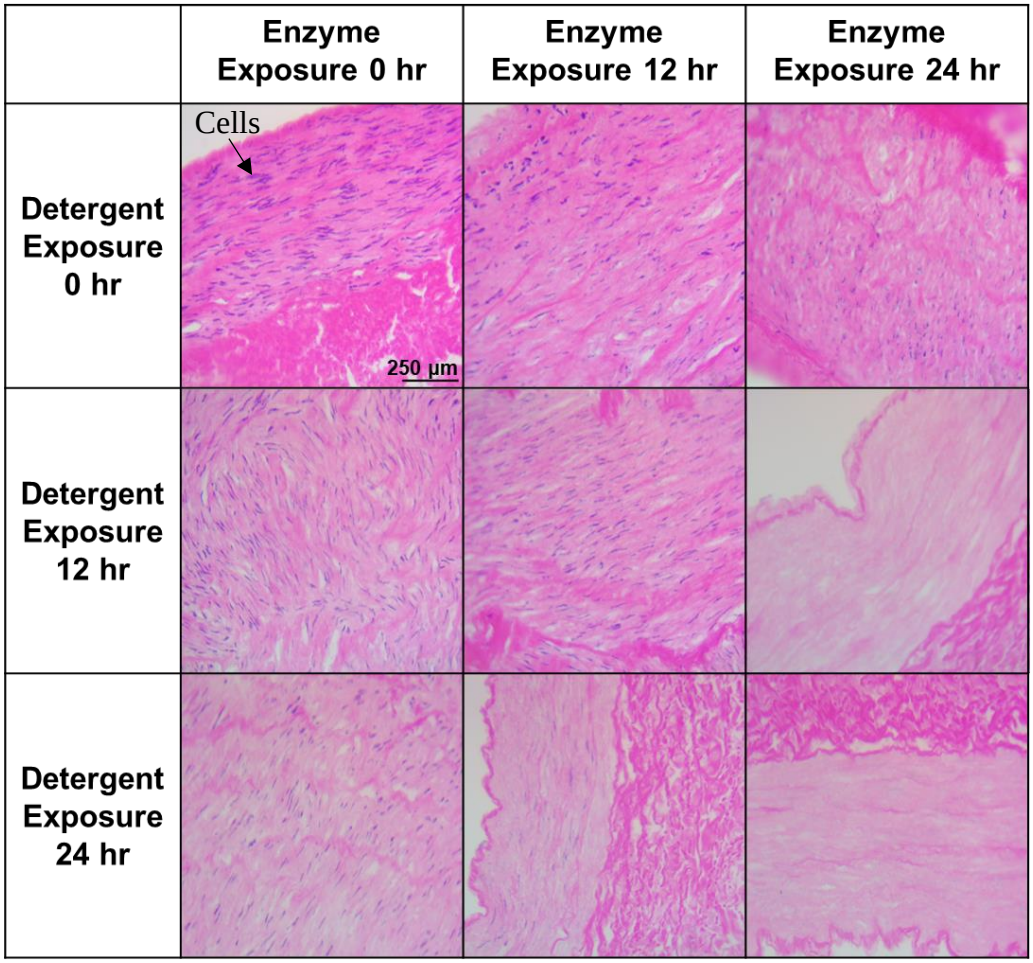

Figure 3-3: 40X magnification of H&E-stained LADA for different exposure times and reagents. The hematoxylin stains cell nuclei purple, and eosin stains the ECM pink.

The resulting images from the Masson's trichrome-stained tissues were compared to determine how the different procedures impacted collagen and muscle fibers. **Figure 3-4** shows the images taken using a light microscope with a 10X objective. The 10X objective was chosen to better visualize the artery layers.

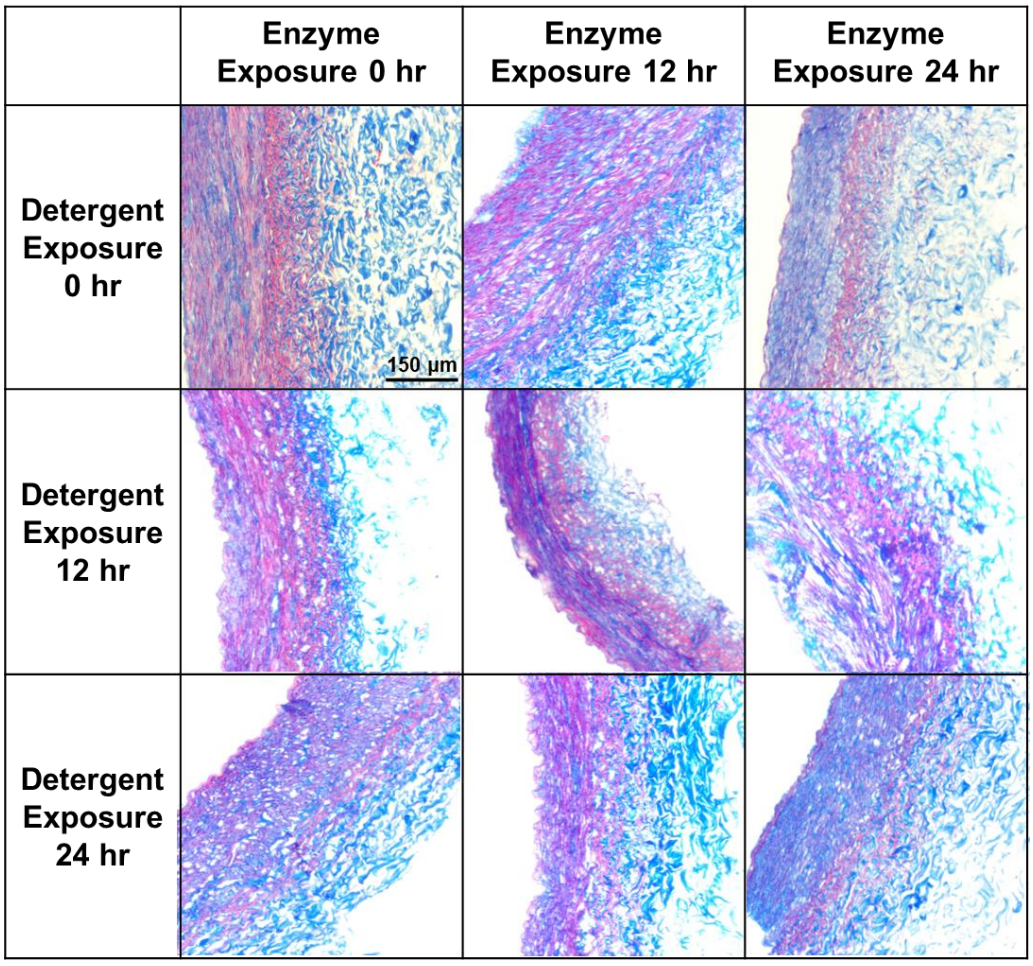

Figure 3-4: 10X magnification of Masson Trichrome stained LADA for different exposure times and reagents. Collagen is stained blue, cell nuclei black/dark purple, and muscle and cytoplasm red/purple.

The resulting images from the EVG-stained tissues were compared to determine how the different procedures impacted elastin, collagen, and muscle fibers. **Figure 3-5** shows the images taken using a light microscope with a 10X objective.

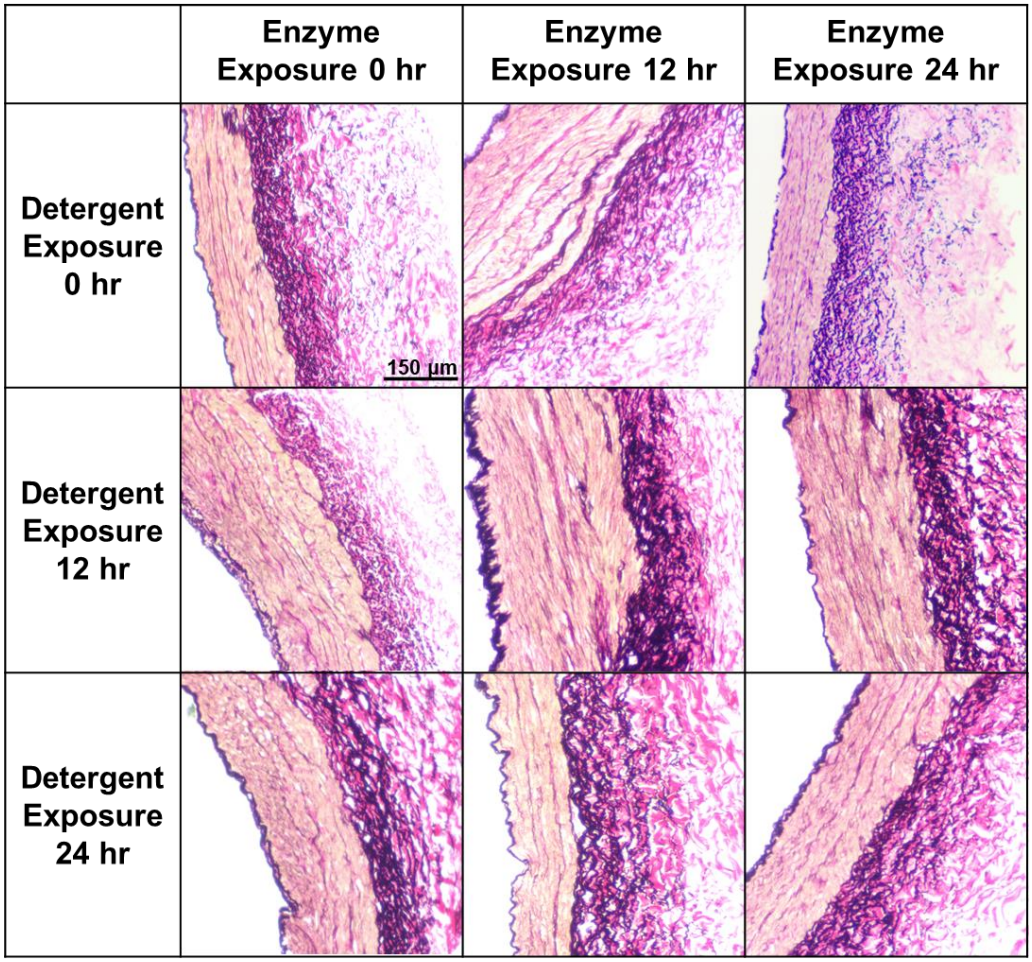

Figure 3-5: 10X magnification of EVG stained LADA for different exposure times and reagents. The elastin is stained dark purple, the collagen is stained red, and muscle is stained yellow.

3.3 Discussion

When choosing the optimal decellularization procedure, the most important consideration is effective cell removal to minimize the risk of adverse immune responses to the graft. To visualize the cells following the different exposure times to the detergent and enzymatic solutions, histological analysis of LADA tissue was performed using H&E. By qualitatively examining the stained tissues for cells, it was revealed that the only protocol that reliably removed all cells in all the replications was the final protocol using 24-hour exposure to detergent followed by 24-hour exposure to the enzyme solution (**Figure 3-3**). Using that information, the optimal decellularized procedure to remove cells was determined to be a 24-hour submersion in Triton X-100, 24-hour submersion in DI water, 24-hour submersion in the enzyme solution, and finally, a 24-hour submersion in PBS.

Another important consideration in decellularization is ensuring the preservation of the ECM. Further histological analysis of the LADA tissue using Masson's trichrome (**Figure 3-4**) and EVG (**Figure 3-5**). Following the application of Masson's trichrome stain, the arterial layers could be differentiated by the purple muscle fibers and the blue collagen. The intensity and distribution of the collagen was not found to be altered in the decellularized tissue (**Figure 3-4**). Furthermore, after the application of the EVG stain, the internal and external elastic lamina and the elastin fibers in the tunica media can be visualized by the purple color in all of the stained tissues (**Figure 3-5**). No degradation of the elastin can be seen in the decellularized tissue. Histological analysis revealed no major qualitative difference in collagen or elastin content between the decellularized tissue and the control. This suggests that the chosen decellularization method effectively removes cellular components without damaging the ECM components.

CHAPTER 4 – MECHANICAL TESTING and pSFDI

While previous research has been done looking into the decellularization of porcine coronary arteries, the impact of decellularization on vessel's mechanical properties and collagen architecture has not been thoroughly explored[29]. Therefore, in this chapter, biaxial mechanical testing and polarized spatial frequency domain imaging (pSFDI) were conducted. The mechanical properties analyzed were low-tension elastic modulus (E^{LT}), high-tension elastic modulus (E^{HT}), tissue extensibility (λ^*), and maximum stretch (λ) for the circumferential and longitudinal directions. E^{LT} and E^{HT} are the slopes of the linear portions of the low- and high-tension regimes of stress-stretch curve, where the first 20% of the data points are fitted to a linear curve for the E^{LT}, and the last 10% of the data points are used for E^{HT}. λ^* is the intercept with the *x*-axis of the E^{HT} linear regression. **Figure 4-1** visually demonstrates E^{LT}, E^{HT}, and λ^* in an anisotropic tissue.

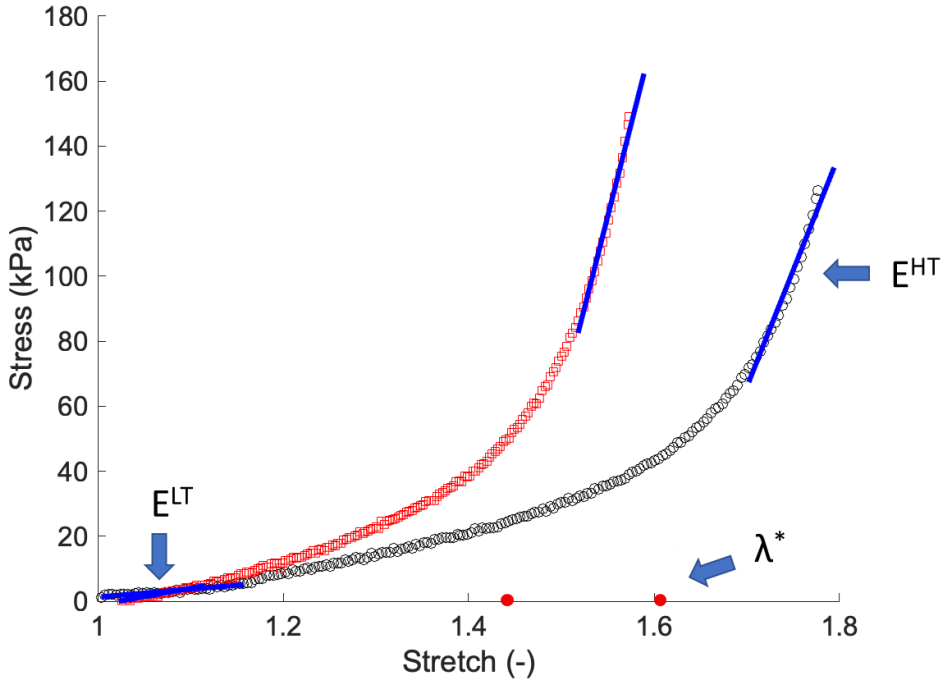

Figure 4-1: Stress-stretch curve in the circumferential and longitudinal directions showing the E^{LT}, E^{HT}, and λ^*.

pSFDI allows for the analysis of collagen fiber orientation at different load dependent states by utilizing birefringent scattering from the collagen fibers in response to light passed through a polarizer. The scattered light is then reflected back through the polarizer, and the intensity of the light is measured. The pSFDI system provides useful information about the collagen architecture through the θ_{fiber}, which is the average angle of a group of collagen fibers, and the degree of optical anisotropy (DOA), which is related to the alignment of collagen fibers. Smaller DOA values indicate a random collagen network, while larger DOA values indicate a more highly aligned collagen network. The maximum intensity occurs when $\theta_{fiber} = \theta_{polarizer}$[30]. The in-house pSFDI system is shown in **Figure 4-2**.

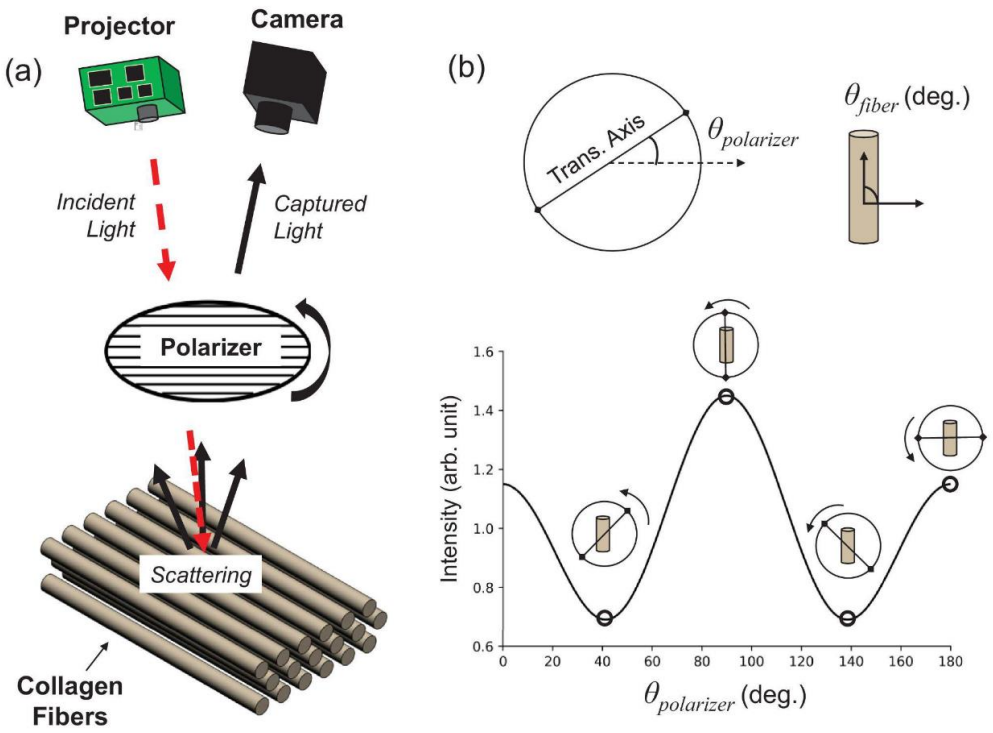

Figure 4-2: pSFDI system set up and mechanism: a) Schematic of the pSFDI system setup; b) Depicts the θ_{fiber} and $\theta_{polarizer}$ as well as the bimodal intensity peak in relation to the $\theta_{polarizer}$ (Image from Jett et al. 2021[30]).

4.1 Methods

In this study, the LADA tissue samples were subjected to biaxial testing and pSFDI before and after decellularization. First, the proximal region of the LADA was cut from the medial and distal portions. Next, a cut was made along the longitudinal axis of the proximal region, and the tissue was laid out in a rectangular shape. A square with an effective testing region of 6mm by 6mm was cut. This sample was then mounted onto a commercial biaxial tester (BioTester, CellScale Biomaterials Testing, Canada) using tines (BioRakes) to pierce the tissue The tissue mounting as well as the preconditioning procedure and loading ratios are depicted in **Figure 4-3**.

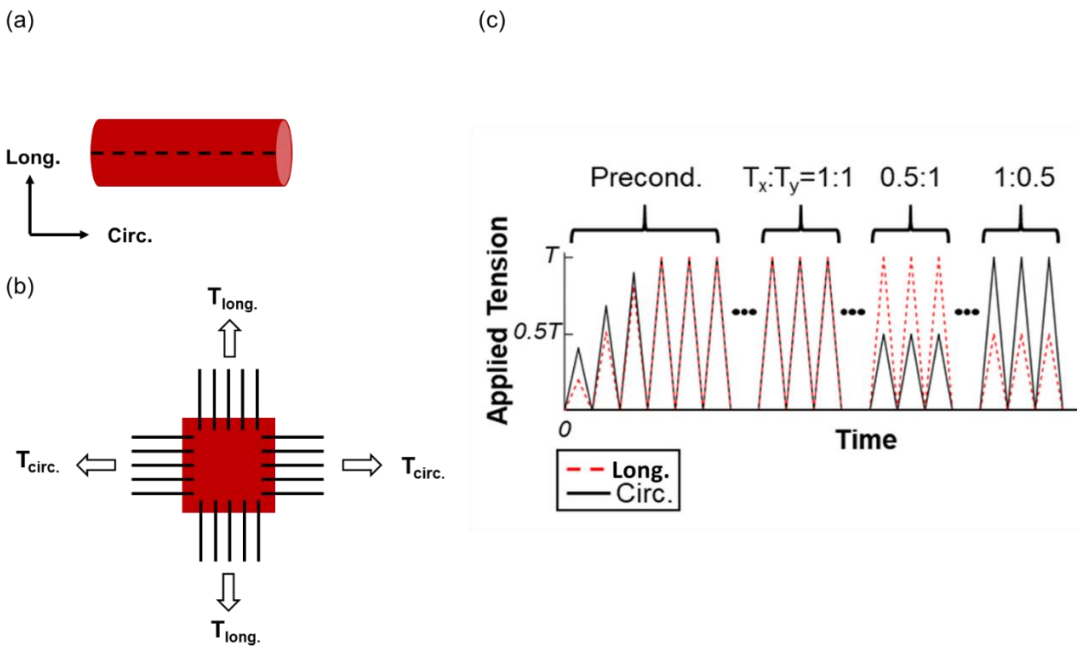

Figure 4-3: Sample preparation for biaxial testing and pSFDI: a) The proximal region of the LADA was cut longitudinally along the dashed line; b) The square tissue sample was cut out and was mounted to the Biotester using four sets of tines; c) The applied tension-time graph demonstrates the preconditioning procedures and the tension ratios tested.

Once mounted, the LADA sample was submerged in a bath of PBS at 32 °C. This temperature was chosen to approximate *in vivo* temperatures while preventing the polarizer from fogging up. First, the samples were subjected to a preconditioning protocol to restore the tissue to its in vivo configuration and to achieve a reproducible state[31]. This preconditioning protocol contained fifteen force-controlled loading-unloading cycles where a targeted first Piola-Kirchhoff (1st PK) stress of 120 kPa was used[7]. Following preconditioning, the biaxial testing protocol performed displacement-controlled tests targeting different 1st PK stress ratios in the tissue's two directions (1:1, 1:0.5, 0.5:1). This procedure was performed before and after treatment with either DI water and PBS for the control group (n=6), or detergent and enzyme

solutions for the test group (n=6). Following treatment, the specimen was mounted with a 5 mm x 5 mm testing region, and preconditioning and biaxial testing were performed again. The reduction in testing region following treatment was done to avoid the puncture marks made by the tines from the previous testing procedure.

In addition to biaxial testing, pSFDI was performed before and after treatment. Images were taken at different polarizer angles for the mounting position, and the peak stretches of the P_{CC}: P_{LL} = 1:1, 1:0.5, and 0.5:1 ratios. The intensity, I, of each pixel was fitted with a three-term Fourier series where α_0 represents the mean light intensity, and α_2 and α_4 represent the polarization-dependent intensity changes. Next, the DOA was calculated to show local collagen fiber dispersion.

$$I = \alpha_0 + \alpha_2\left[2\left(\theta_{fiber} - \theta_{polarizer}\right)\right] + \alpha_4[4((\theta_{fiber} - \theta_{polarizer})] \quad (4.1)$$

Next, the DOA is calculated to show local collagen fiber dispersion.

$$\text{DOA} = \frac{\alpha_2+\alpha_4}{\alpha_0+\alpha_2+\alpha_4} \quad (4.2)$$

4.2 Results

For the following loading ratios (P_{CC}: P_{LL} = 1:1, 1:0.5, and 0.5:1), the pre-treatment and post-treatment circumferential E^{HT} (kPa) was compared for the control and decellularized tissues. A paired *t*-test was performed between the pre-treatment and post-treatment values. There was no statistical significance found for any of the loading ratios between the pre-treatment and post-treatment values for either the control or decellularized groups. This is shown in **Figure 4-6**.

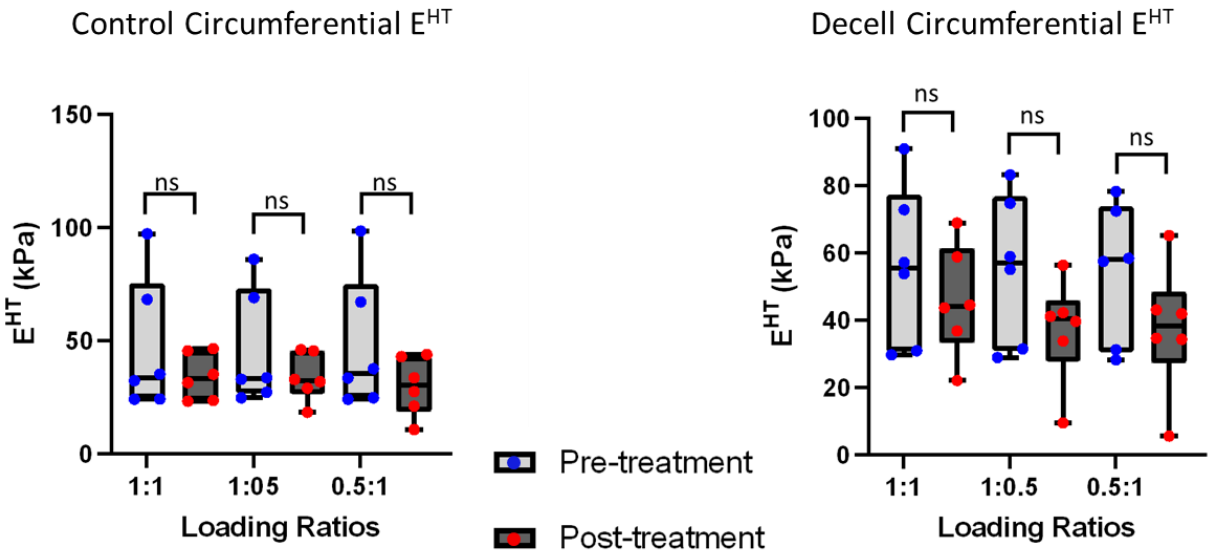

Figure 4-6: Circumferential E^{HT} (kPa) pre- and post-treatment for control (left) and decellularized tissue (right) at different loading ratios. Pre-treatment values are compared to post-treatment values with a paired *t*-test. Statistical significance is indicated with * = $p < 0.05$, ** = $p < 0.005$, and ns = not statistically significant ($p \geq 0.05$).

For the following loading ratios (P_{CC}: P_{LL} = 1:1, 1:0,5, and 0.5:1), the post-treatment circumferential E^{HT} (kPa) of the control and decellularized groups were compared using an unpaired *t*-test. There was no statistical significance found for any of the loading ratios between the post-treatment values for the control and decellularized groups. This is shown in **Figure 4-7**.

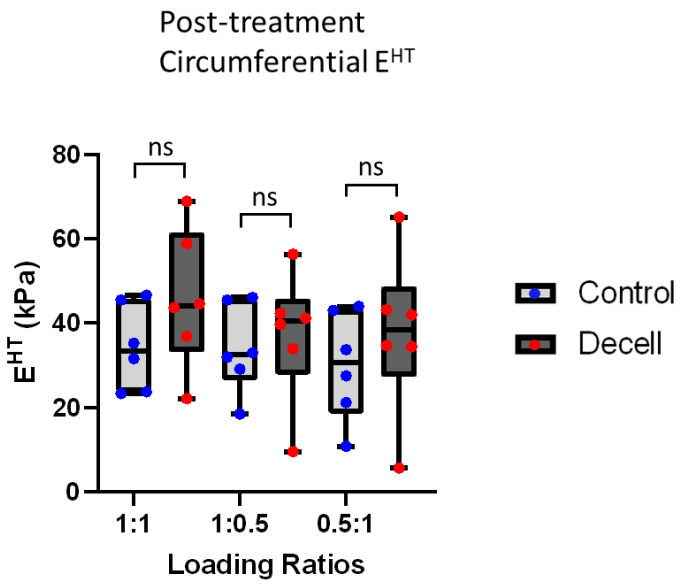

Figure 4-7: Post-treatment circumferential E^{HT} (kPa) for control and decellularized tissues at different loading ratios are compared with an unpaired *t*-test. Statistical significance is indicated with * = $p < 0.05$, ** = $p < 0.005$, and ns = not statistically significant ($p \geq 0.05$).

For the following loading ratios (P_{CC}: P_{LL} = 1:1, 1:0.5, and 0.5:1), the pre-treatment and post-treatment longitudinal E^{HT} (kPa) was compared for the control and decellularized tissues. A paired *t*-test was performed between the pre-treatment and post-treatment values. There was statistical significance found for all the loading ratios between the pre-treatment and post-treatment values for the control group, however, there was no statistical difference between the pre-treatment and post-treatment values for decellularized group. This is shown in **Figure 4-8.**

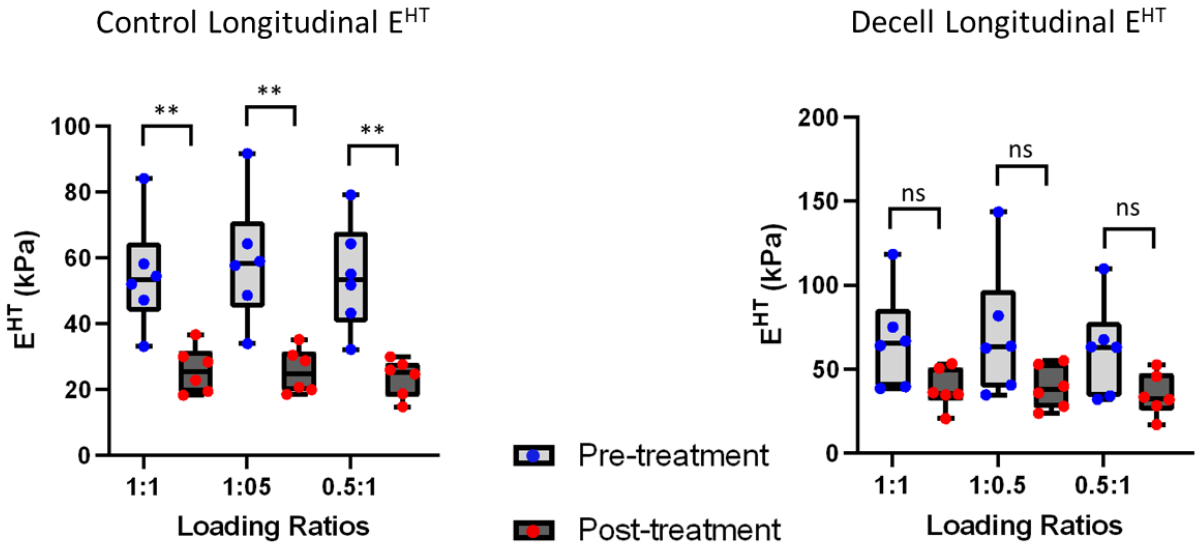

Figure 4-8: Longitudinal E^{HT} (kPa) pre- and post-treatment for control (left) and decellularized tissue (right) at different loading ratios. Pre-treatment values are compared to post-treatment values with a paired *t*-test. Statistical significance is indicated with * = $p < 0.05$, ** = $p < 0.005$, and ns = not statistically significant ($p \geq 0.05$).

For the following loading ratios (P_{CC}: P_{LL} = 1:1, 1:0,5, and 0.5:1), the post-treatment longitudinal E^{HT} (kPa) of the control and decellularized groups were compared using an unpaired *t*-test. There was a statistically significant difference found between the post-treatment values for the control and decellularized groups in the 1:05 ratios, but not in the 1:1 or 0.5:1 ratios. This is shown in **Figure 4-9**.

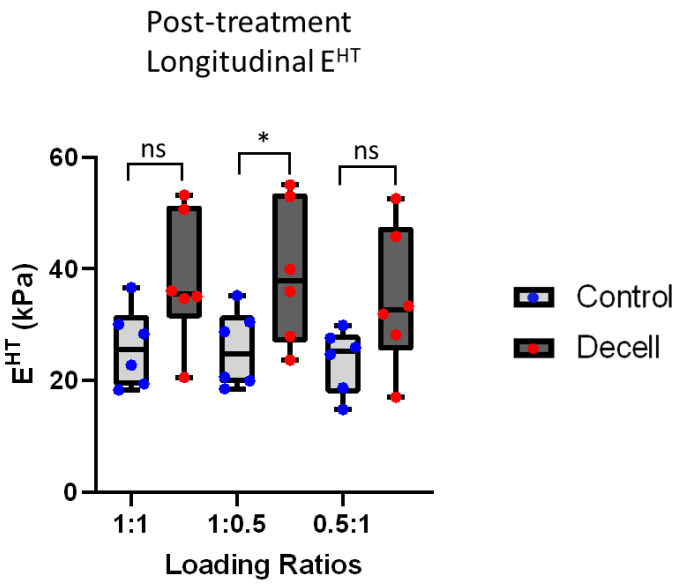

Figure 4-9: Post-treatment longitudinal E^{HT} (kPa) for control and decellularized tissues at different loading ratios are compared with an unpaired *t*-test. Statistical significance is indicated with * = $p < 0.05$, ** = $p < 0.005$, and ns = not statistically significant ($p \geq 0.05$).

The circumferential and longitudinal E^{HT} values for the control and decellularized tissues were recorded, and the mean values were calculated. The percent change was calculated between the pre-treatment and post-treatment values. This is shown in **Table 4-1** through **Table 4-4**.

Table 4-1: Circumferential E^{HT} (kPa) for control tissues

Circumferential EHT Control								
	Tissue 1	**Tissue 2**	**Tissue 3**	**Tissue 4**	**Tissue 5**	**Tissue 6**	**Mean ± SD**	**% Change**
1:1 Pre-treatment	97.3	24.1	24.3	35.3	32.4	68.3	47.0±29.6	-26.95%
1:1 Post-treatment	46.6	35.2	31.5	23.7	23.3	45.5	34.3±10.2	
1:0.5 Pre-treatment	86.0	24.9	27.3	33.0	33.6	69.1	45.6±25.5	-25.48%
1:0.5 Post-treatment	46.1	31.9	33.0	18.4	29.1	45.5	34.0±10.5	
0.5:1 Pre-treatment	98.5	24.9	24.1	37.7	33.6	67.2	47.7±29.5	-37.02%
0.5:1 Post-treatment	44.0	33.7	27.5	21.1	10.8	43.0	30.0±12.9	

Table 4-2: Circumferential E^{HT} (kPa) for decellularized tissues

Circumferential EHT Decell								
	Tissue 1	**Tissue 2**	**Tissue 3**	**Tissue 4**	**Tissue 5**	**Tissue 6**	**Mean ± SD**	**% Change**
1:1 Pre-treatment	57.2	90.9	31.0	29.8	53.9	72.8	55.9±23.8	-18.03%
1:1 Post-treatment	36.9	44.6	68.9	22.1	58.9	43.7	45.8±16.5	
1:0.5 Pre-treatment	59.0	83.2	31.5	29.0	55.1	74.8	55.4±22.0	-32.95%
1:0.5 Post-treatment	33.9	39.7	41.2	9.5	56.4	42.3	37.2±15.5	
0.5:1 Pre-treatment	57.5	78.3	28.3	31.3	58.5	72.5	54.4±20.7	-31.03%
0.5:1 Post-treatment	34.7	42.0	34.4	5.6	65.2	43.2	37.5±19.3	

Table 4-3: Longitudinal E^{HT} (kPa) for control tissues

Longitudinal EHT Control								
	Tissue 1	**Tissue 2**	**Tissue 3**	**Tissue 4**	**Tissue 5**	**Tissue 6**	**Mean ± SD**	**% Change**
1:1 Pre-treatment	58.2	33.1	52.1	84.2	54.5	47.2	54.9±16.8	-52.72%
1:1 Post-treatment	19.4	22.8	30.1	36.7	28.4	18.3	25.9±7.1	
1:0.5 Pre-treatment	57.7	34.0	58.9	91.7	64.3	48.6	59.2±19.2	-56.76%
1:0.5 Post-treatment	20.7	20.0	28.8	35.2	30.5	18.5	25.6±6.8	
0.5:1 Pre-treatment	64.3	32.2	51.8	79.1	55.2	43.2	54.3±16.3	-56.47%
0.5:1 Post-treatment	24.7	18.7	27.6	29.9	26.0	14.8	23.6±5.7	

Table 4-4: Longitudinal E^{HT} (kPa) for decellularized tissues

Longitudinal EHT Decell								
	Tissue 1	**Tissue 2**	**Tissue 3**	**Tissue 4**	**Tissue 5**	**Tissue 6**	**Mean ± SD**	**% Change**
1:1 Pre-treatment	66.7	118.5	38.6	64.1	75.1	39.7	67.1±29.2	-42.79%
1:1 Post-treatment	53.2	20.6	35.1	36.1	50.7	34.7	38.4±12.0	
1:0.5 Pre-treatment	62.5	143.6	40.6	63.8	81.7	34.7	71.2±39.4	-44.84%
1:0.5 Post-treatment	53.0	23.7	39.9	27.9	55.1	36.0	39.3±12.8	
0.5:1 Pre-treatment	63.0	109.7	32.0	63.3	67.5	34.1	61.6±28.2	-43.46%
0.5:1 Post-treatment	52.6	17.0	33.4	28.2	45.8	31.9	34.8±12.7	

For the following loading ratios (P_{CC}: P_{LL} = 1:1, 1:0.5, and 0.5:1), the pre-treatment and post-treatment circumferential E^{LT} (kPa) was compared for the control and decellularized tissues. A paired *t*-test was performed between the pre-treatment and post-treatment values. There was statistical significance found for all of the loading ratios between the pre-treatment and post-treatment values for both the control group and the decellularized group. This is shown in **Figure 4-10**.

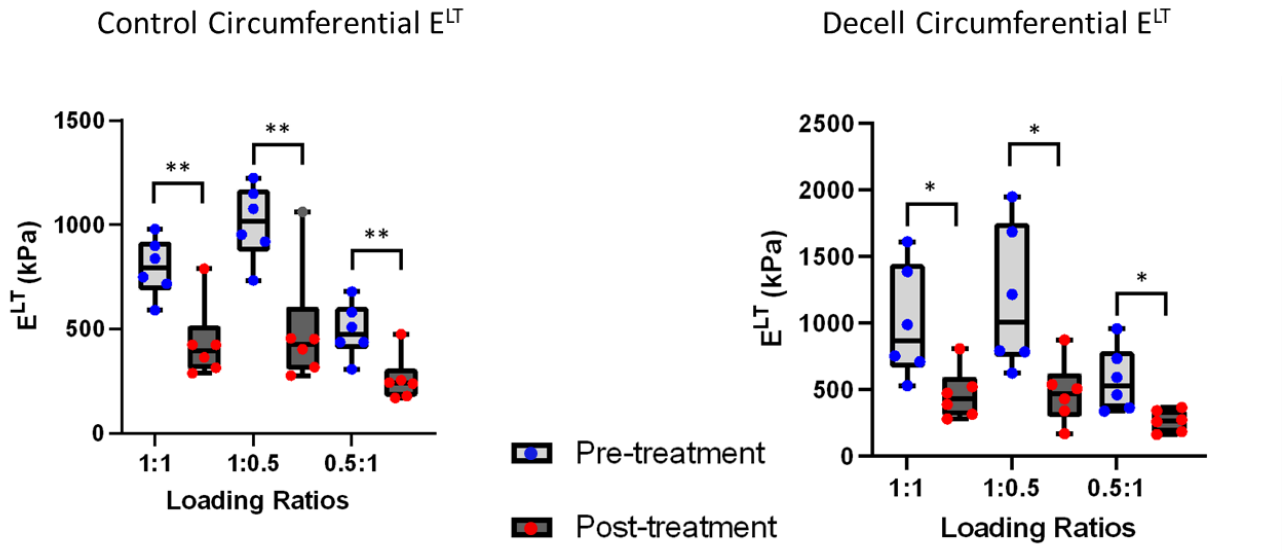

Figure 4-10: Circumferential E^{LT} (kPa) pre- and post-treatment for control (left) and decellularized tissue (right) at different loading ratios. Pre-treatment values are compared to post-treatment values with a paired *t*-test. Statistical significance is indicated with * = $p < 0.05$, ** = $p < 0.005$, and ns = not statistically significant ($p \geq 0.05$).

For the following loading ratios (P_{CC}: P_{LL} = 1:1, 1:0,5, and 0.5:1), the post-treatment circumferential E^{LT} (kPa) of the control and decellularized groups were compared using an unpaired *t*-test. There was no statistical significance found for any of the loading ratios between the post-treatment values for the control and decellularized groups, as shown in **Figure 4-11**.

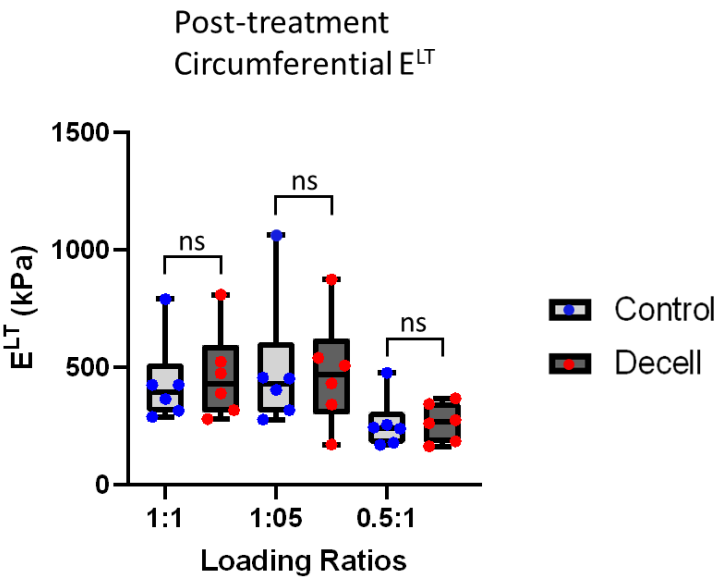

Figure 4-11: Post-treatment circumferential E^{LT} (kPa) for control and decellularized tissues at different loading ratios are compared with an unpaired *t*-test. Statistical significance is indicated with * = $p < 0.05$, ** = $p < 0.005$, and ns = not statistically significant ($p \geq 0.05$).

For the following loading ratios (P_{CC}: P_{LL} = 1:1, 1:0.5, and 0.5:1), the pre-treatment and post-treatment longitudinal E^{LT} (kPa) was compared for the control and decellularized tissues. A paired *t*-test was performed between the pre-treatment and post-treatment values. There was statistical significance found for all the loading ratios between the pre-treatment and post-treatment values for both the control group and the decellularized group. This is shown in **Figure 4-12**.

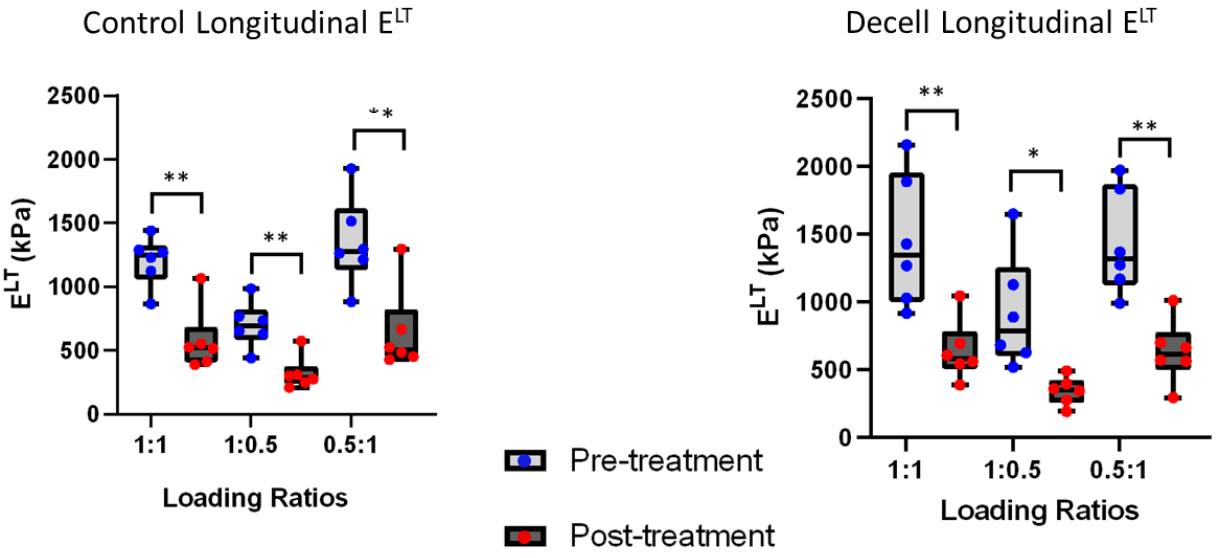

Figure 4-12: Longitudinal E^{LT} (kPa) pre and post-treatment for control (left) and decellularized tissue (right) at different loading ratios. Pre-treatment values are compared to post-treatment values with a paired *t*-test. Statistical significance is indicated with * = $p < 0.05$, and ** = $p < 0.005$.

For the following loading ratios (P_{CC}: P_{LL} = 1:1, 1:0,5, and 0.5:1), the post-treatment longitudinal E^{LT} (kPa) of the control and decellularized groups were compared using an unpaired *t*-test. There was no statistical significance found for any of the loading ratios between the post-treatment values for the control and decellularized groups. This is shown in **Figure 4-13**.

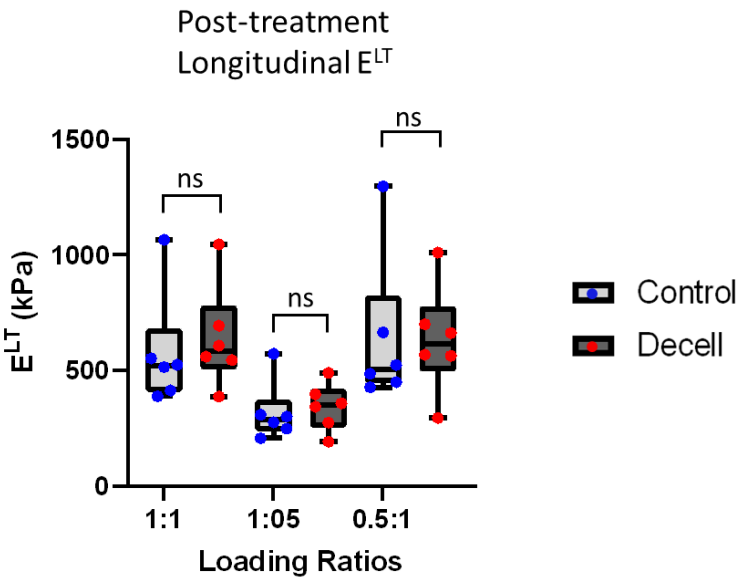

Figure 4-13: Post-treatment longitudinal E^{LT} (kPa) for control and decellularized tissues at different loading ratios are compared with an unpaired *t*-test. Statistical significance is indicated with * = $p < 0.05$, ** = $p < 0.005$, and ns = not statistically significant ($p \geq 0.05$).

The circumferential and longitudinal E^{LT} values for the control and decellularized tissues were recorded, and the mean values were calculated. The percent change was calculated between the pre-treatment and post-treatment values. This is shown in **Table 4-5** through **Table 4-8**.

Table 4-5: Circumferential E^{LT} (kPa) for control tissues

Circumferential ELT Control								
	Tissue 1	**Tissue 2**	**Tissue 3**	**Tissue 4**	**Tissue 5**	**Tissue 6**	**Mean ± SD**	**% Change**
1:1 Pre-treatment	838.4	590.0	717.0	979.2	899.5	749.2	795.6±139.2	-45.43%
1:1 Post-treatment	789.6	314.2	364.2	288.4	424.0	424.7	434.2±182.8	
1:0.5 Pre-treatment	1077.5	732.6	953.5	1224.1	1149.6	919.8	1009.5±177.8	-51.04%
1:0.5 Post-treatment	1061.5	316.6	455.3	276.8	452.3	403.0	494.2±287.1	
0.5:1 Pre-treatment	679.6	306.9	437.2	580.2	509.9	436.6	491.7±129.3	-47.19%
0.5:1 Post-treatment	475.2	169.6	237.6	178.0	243.6	254.0	259.7±111.4	

Table 4-6: Circumferential E^{LT}(kPa) for decellularized tissues

Circumferential ELT Decell								
	Tissue 1	**Tissue 2**	**Tissue 3**	**Tissue 4**	**Tissue 5**	**Tissue 6**	**Mean ± SD**	**% Change**
1:1 Pre-treatment	1385.7	1612.1	531.2	988.1	710.3	753.2	996.8±421.5	-53.38%
1:1 Post-treatment	807.6	522.9	388.5	279.5	473.3	316.4	464.7±191.4	
1:0.5 Pre-treatment	1687.4	1949.4	624.0	1216.0	793.1	784.1	1175.7±541.5	-59.45%
1:0.5 Post-treatment	873.1	538.9	431.2	170.5	506.8	340.2	476.8±235.1	
0.5:1 Pre-treatment	733.6	956.6	339.1	593.2	460.9	364.6	574.7±238.4	-53.85%
0.5:1 Post-treatment	366.5	343.5	274.0	163.4	260.1	183.8	265.2±81.8	

Table 4-7: Longitudinal E^{LT} (kPa) for control tissues

Longitudinal ELT Control								
	Tissue 1	**Tissue 2**	**Tissue 3**	**Tissue 4**	**Tissue 5**	**Tissue 6**	**Mean ± SD**	**% Change**
1:1 Pre-treatment	1269.7	865.8	1123.0	1287.7	1229.5	1441.4	1202.9±194.5	-52.01%
1:1 Post-treatment	1066.2	389.2	553.0	414.3	515.7	525.0	577.2±248.2	
1:0.5 Pre-treatment	629.7	441.2	652.8	983.6	766.8	736.4	701.8±179.1	-54.44%
1:0.5 Post-treatment	573.6	208.4	309.4	249.1	276.3	301.4	319.7±129.7	
0.5:1 Pre-treatment	1928.6	882.9	1213.7	1295.0	1263.3	1515.3	1349.8±349.1	-52.42%
0.5:1 Post-treatment	1297.1	450.8	665.9	428.5	523.9	487.0	642.2±331.6	

Table 4-8: Longitudinal E^{LT} (kPa) for decellularized tissues

Longitudinal ELT Decell								
	Tissue 1	**Tissue 2**	**Tissue 3**	**Tissue 4**	**Tissue 5**	**Tissue 6**	**Mean ± SD**	**% Change**
1:1 Pre-treatment	1888.6	2160.1	918.0	1267.9	1029.0	1427.4	1448.5±488.0	-55.8%
1:1 Post-treatment	1045.7	545.3	607.6	388.5	694.4	560.8	640.4±222.3	
1:0.5 Pre-treatment	1127.3	1648.2	519.2	888.7	626.3	682.1	915.3±419.0	-62.5%
1:0.5 Post-treatment	490.6	359.6	345.0	192.9	397.7	275.3	343.5±102.2	
0.5:1 Pre-treatment	1834.0	1971.3	989.9	1273.9	1169.2	1367.6	1434.3±386.3	-55.81%
0.5:1 Post-treatment	1011.0	663.0	569.0	295.4	700.7	563.9	633.8±232.9	

For the following loading ratios (P_{CC}: P_{LL} = 1:1, 1:0.5, and 0.5:1), the pre-treatment and post-treatment circumferential λ^* was compared for the control and decellularized tissues. A paired *t*-test was performed between the pre-treatment and post-treatment values. There was statistical significance found for all the loading ratios between the pre-treatment and post-treatment values for both the control group and the decellularized group. This is shown in **Figure 4-14**.

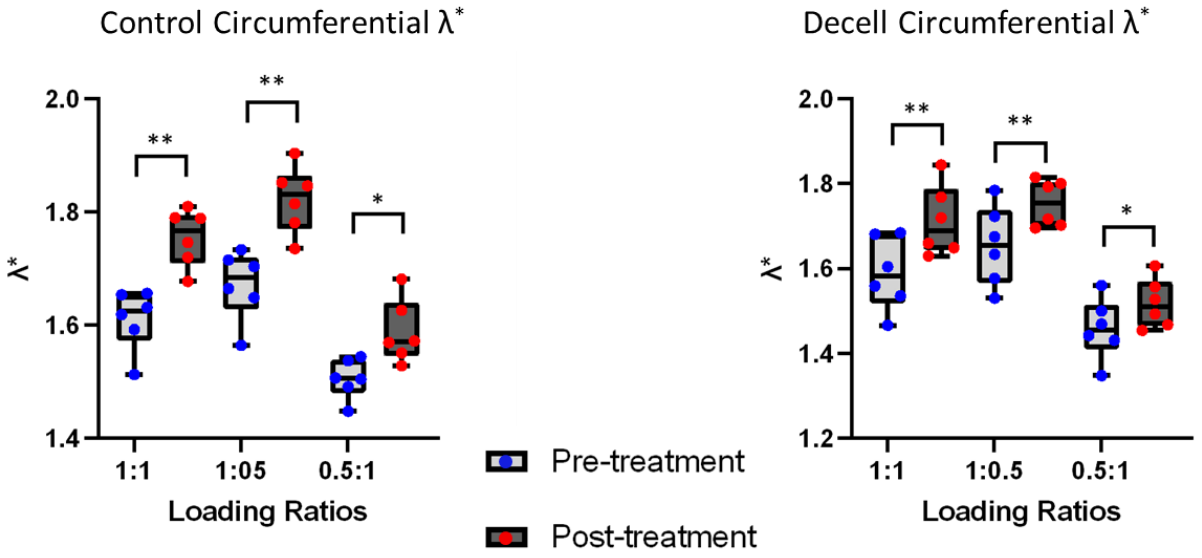

Figure 4-14: Circumferential λ^* pre- and post-treatment for control (left) and decellularized tissue (right) at different loading ratios. Pre-treatment values are compared to post-treatment values with a paired *t*-test. Statistical significance is indicated with * = $p < 0.05$, ** = $p < 0.005$, and ns = not statistically significant ($p \geq 0.05$).

For the following loading ratios (P_{CC}: P_{LL} = 1:1, 1:0,5, and 0.5:1), the post-treatment circumferential λ^* of the control and decellularized groups were compared using an unpaired *t*-test. There was no statistical significance found for any of the loading ratios between the post-treatment values for the control and decellularized groups. This is shown in **Figure 4-15**.

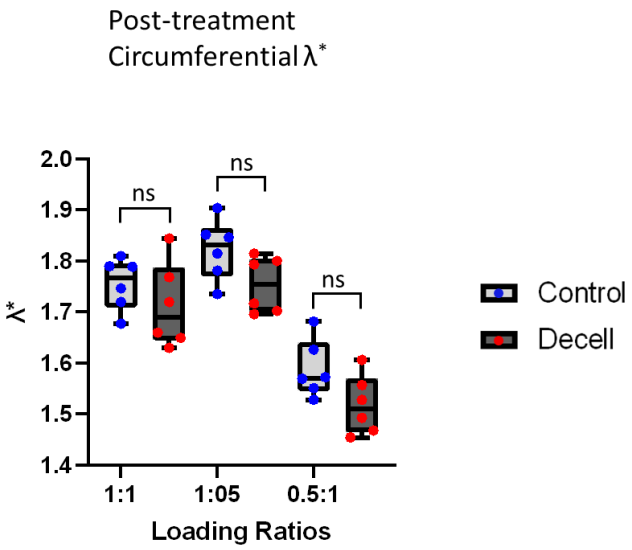

Figure 4-15: Post-treatment circumferential λ^* for control and decellularized tissues at different loading ratios are compared with an unpaired *t*-test. Statistical significance is indicated with * = $p < 0.05$, ** = $p < 0.005$, and ns = not statistically significant ($p \geq 0.05$).

For the following loading ratios (P_{CC}: P_{LL} = 1:1, 1:0.5, and 0.5:1), the pre-treatment and post-treatment longitudinal λ^* was compared for the control and decellularized tissues. A paired *t*-test was performed between the pre-treatment and post-treatment values. There was statistical significance found for most of the loading ratios between the pre-treatment and post-treatment values for both the control group and the decellularized group. This is shown in **Figure 4-16**.

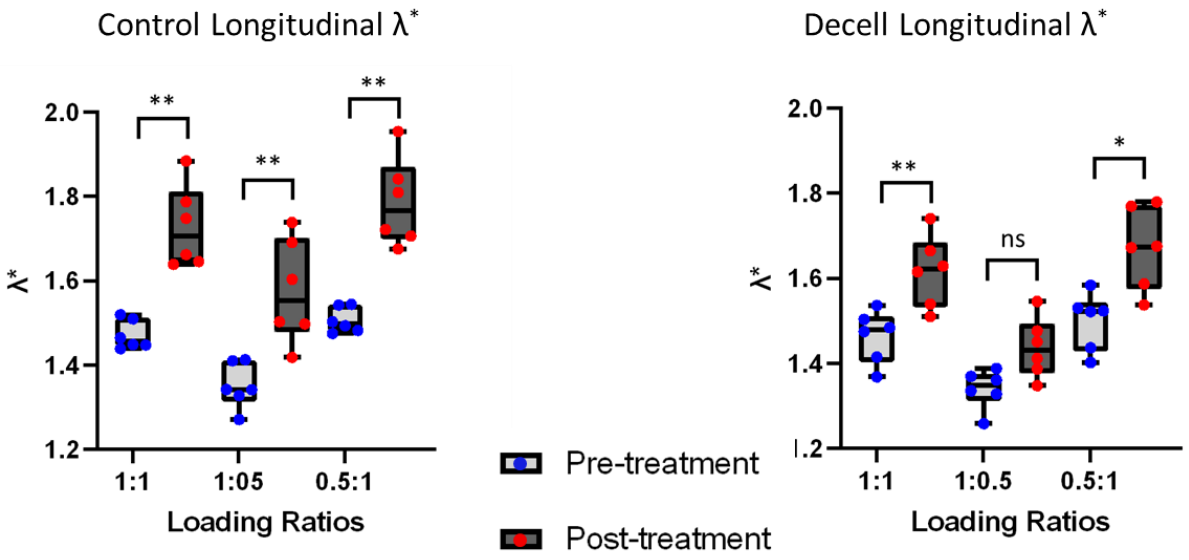

Figure 4-16: Longitudinal λ^* pre- and post-treatment for control (left) and decellularized tissue (right) at different loading ratios. Pre-treatment values are compared to post-treatment values with a paired *t*-test. Statistical significance is indicated with * = $p < 0.05$, ** = $p < 0.005$, and ns = not statistically significant ($p \geq 0.05$).

For the following loading ratios (P_{CC}: P_{LL} = 1:1, 1:0,5, and 0.5:1), the post-treatment longitudinal λ^* of the control and decellularized groups were compared using an unpaired *t*-test. There was no statistical significance found for the 1:1 and 0.5:1 ratios between the post-treatment values for the control and decellularized groups; however, there was a statistically significant different between the post-treatment values in the 1:0.5 ratio. This is shown in **Figure 4-17**.

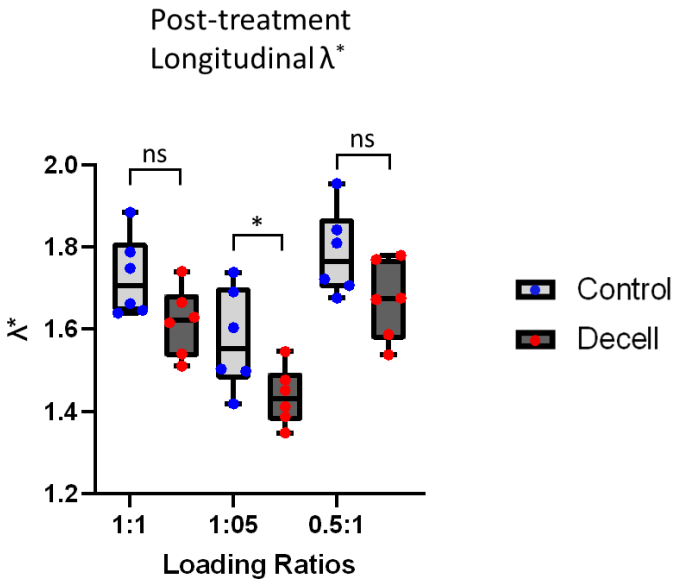

Figure 4-17: Post-treatment longitudinal λ^* for control and decellularized tissues at different loading ratios are compared with an unpaired *t*-test. Statistical significance is indicated with * = $p < 0.05$, ** = $p < 0.005$, and ns = not statistically significant ($p \geq 0.05$).

The circumferential and longitudinal λ^* values for the control and decellularized tissues were recorded, and the mean values were calculated. The percent change was calculated between the pre-treatment and post-treatment values. This is shown in **Table 4-9** through **Table 4-12**.

Table 4-9: Circumferential λ^*values for control tissues.

Circumferential Extensibility Control								
	Tissue 1	**Tissue 2**	**Tissue 3**	**Tissue 4**	**Tissue 5**	**Tissue 6**	**Mean ± SD**	**% Change**
1:1 Pre-treatment	1.513	1.619	1.631	1.656	1.592	1.654	1.611±0.054	8.97%
1:1 Post-treatment	1.790	1.746	1.720	1.810	1.677	1.789	1.760±0.050	
1:0.5 Pre-treatment	1.564	1.665	1.704	1.733	1.649	1.715	1.670±0.061	9.00%
1:0.5 Post-treatment	1.852	1.781	1.815	1.904	1.735	1.846	1.820±0.059	
0.5:1 Pre-treatment	1.448	1.491	1.537	1.544	1.507	1.505	1.510±0.035	5.48%
0.5:1 Post-treatment	1.681	1.551	1.569	1.626	1.528	1.572	1.590±0.056	

Table 4-10: Circumferential λ^* values for decellularized tissues.

Circumferential Extensibility Decell								
	Tissue 1	**Tissue 2**	**Tissue 3**	**Tissue 4**	**Tissue 5**	**Tissue 6**	**Mean ± SD**	**% Change**
1:1 Pre-treatment	1.536	1.466	1.604	1.684	1.559	1.681	1.588±0.085	7.78%
1:1 Post-treatment	1.649	1.660	1.768	1.844	1.630	1.720	1.712±0.083	
1:0.5 Pre-treatment	1.577	1.530	1.675	1.784	1.634	1.723	1.654±0.094	6.04%
1:0.5 Post-treatment	1.696	1.717	1.800	1.815	1.702	1.793	1.754±0.054	
0.5:1 Pre-treatment	1.442	1.348	1.469	1.560	1.431	1.500	1.459±0.071	4.04%
0.5:1 Post-treatment	1.528	1.468	1.557	1.606	1.454	1.493	1.518±0.058	

Table 4-11: Longitudinal λ^* values for control tissues.

Longitudinal Extensibility Control								
	Tissue 1	**Tissue 2**	**Tissue 3**	**Tissue 4**	**Tissue 5**	**Tissue 6**	**Mean ± SD**	**% Change**
1:1 Pre-treatment	1.449	1.520	1.465	1.439	1.448	1.510	1.472±0.034	17.42%
1:1 Post-treatment	1.788	1.748	1.645	1.662	1.639	1.884	1.728±0.097	
1:0.5 Pre-treatment	1.328	1.413	1.342	1.271	1.342	1.410	1.351±0.054	16.61%
1:0.5 Post-treatment	1.691	1.603	1.498	1.418	1.503	1.738	1.575±0.124	
0.5:1 Pre-treatment	1.503	1.544	1.494	1.482	1.475	1.543	1.507±0.030	18.46%
0.5:1 Post-treatment	1.842	1.810	1.707	1.722	1.676	1.954	1.785±0.104	

Table 4-12: Longitudinal λ^* values for decellularized tissues.

Longitudinal Extensibility Decell								
	Tissue 1	**Tissue 2**	**Tissue 3**	**Tissue 4**	**Tissue 5**	**Tissue 6**	**Mean ± SD**	**% Change**
1:1 Pre-treatment	1.415	1.368	1.484	1.536	1.475	1.504	1.464±0.062	10.46%
1:1 Post-treatment	1.510	1.665	1.629	1.741	1.540	1.616	1.617±0.084	
1:0.5 Pre-treatment	1.328	1.258	1.370	1.361	1.336	1.389	1.340±0.046	7.18%
1:0.5 Post-treatment	1.347	1.546	1.477	1.412	1.387	1.451	1.437±0.070	
0.5:1 Pre-treatment	1.437	1.402	1.521	1.584	1.524	1.530	1.500±0.067	11.36%
0.5:1 Post-treatment	1.537	1.769	1.676	1.779	1.587	1.672	1.670±0.096	

For the following loading ratios (P_{CC}: P_{LL} = 1:1, 1:0.5, and 0.5:1), the pre-treatment and post-treatment circumferential maximum λ was compared for the control and decellularized tissues. A paired *t*-test was performed between the pre-treatment and post-treatment values. There was statistical significance found for all of the loading ratios between the pre-treatment and post-treatment values for both the control group and the decellularized group. This is shown in **Figure 4-18**.

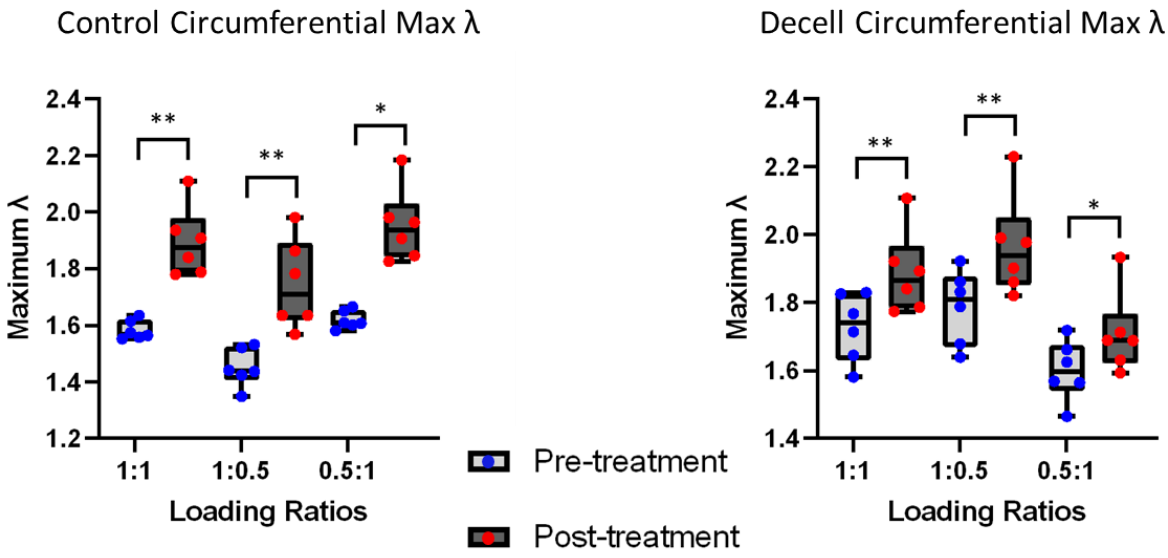

Figure 4-18: Circumferential maximum λ pre- and post-treatment for control (left) and decellularized tissue (right) at different loading ratios. Pre-treatment values are compared to post-treatment values with a paired *t*-test. Statistical significance is indicated with * = $p < 0.05$, ** = $p < 0.005$, and ns = not statistically significant ($p \geq 0.05$).

For the following loading ratios (P_{CC}: P_{LL} = 1:1, 1:0,5, and 0.5:1), the post-treatment circumferential maximum λ of the control and decellularized groups were compared using an unpaired *t*-test. There was no statistical significance found for any of the loading ratios between the post-treatment values for the control and decellularized groups. This is shown in **Figure 4-19**.

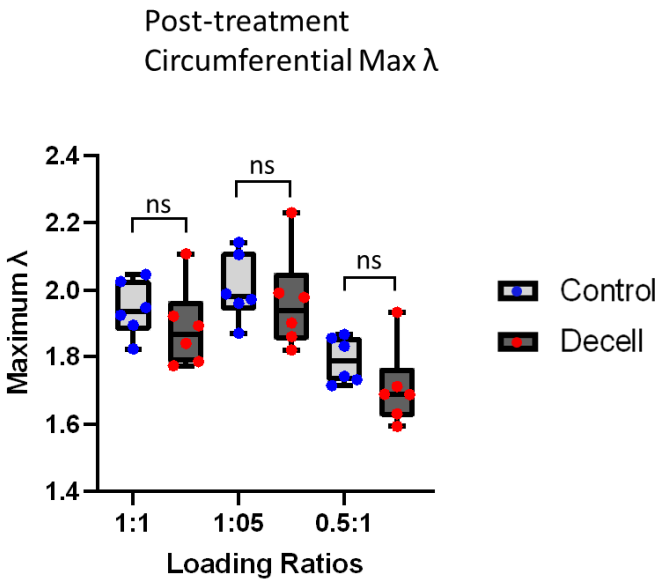

Figure 4-19: Post-treatment circumferential maximum λ for control and decellularized tissues at different loading ratios are compared with an unpaired *t*-test. Statistical significance is indicated with * = $p < 0.05$, ** = $p < 0.005$, and ns = not statistically significant ($p \geq 0.05$).

For the following loading ratios (P_{CC}: P_{LL} = 1:1, 1:0.5, and 0.5:1), the pre-treatment and post-treatment longitudinal maximum λ was compared for the control and decellularized tissues. A paired *t*-test was performed between the pre-treatment and post-treatment values. There was statistical significance found for all of the loading ratios between the pre-treatment and post-treatment values for both the control group and the decellularized group. This is shown in **Figure 4-20**.

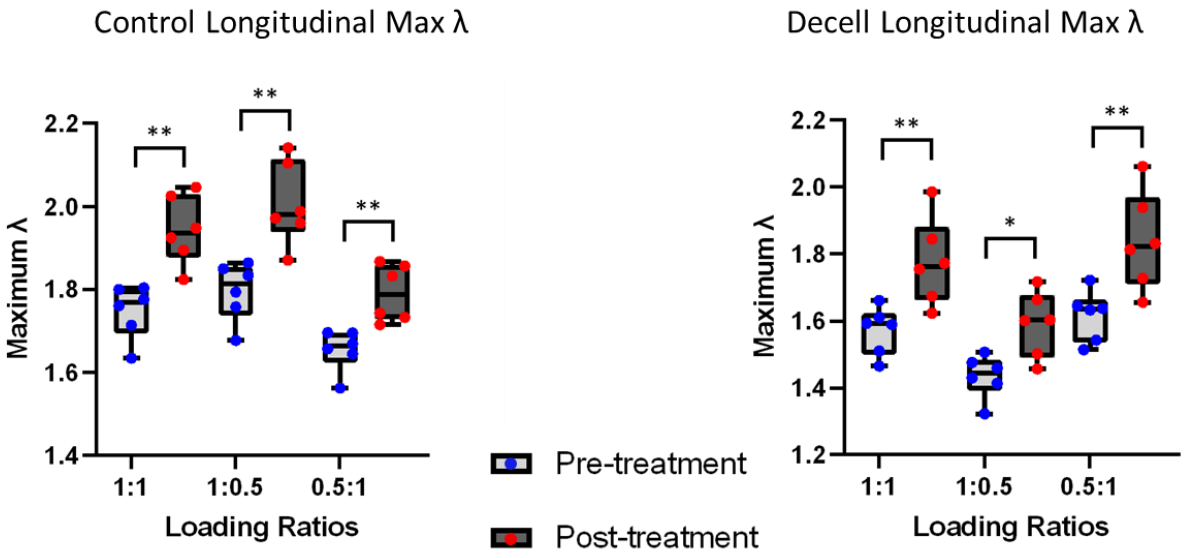

Figure 4-20: Longitudinal maximum λ pre- and post-treatment for control (left) and decellularized tissue (right) at different loading ratios. Pre-treatment values are compared to post-treatment values with a paired *t*-test. Statistical significance is indicated with * = $p < 0.05$, ** = $p < 0.005$, and ns = not statistically significant ($p \geq 0.05$).

For the following loading ratios (P_{CC}: P_{LL} = 1:1, 1:0,5, and 0.5:1), the post-treatment longitudinal maximum λ of the control and decellularized groups were compared using an unpaired *t*-test. There was no statistical significance found for any of the loading ratios between the post-treatment values for the control and decellularized groups. This is shown in **Figure 4-21**.

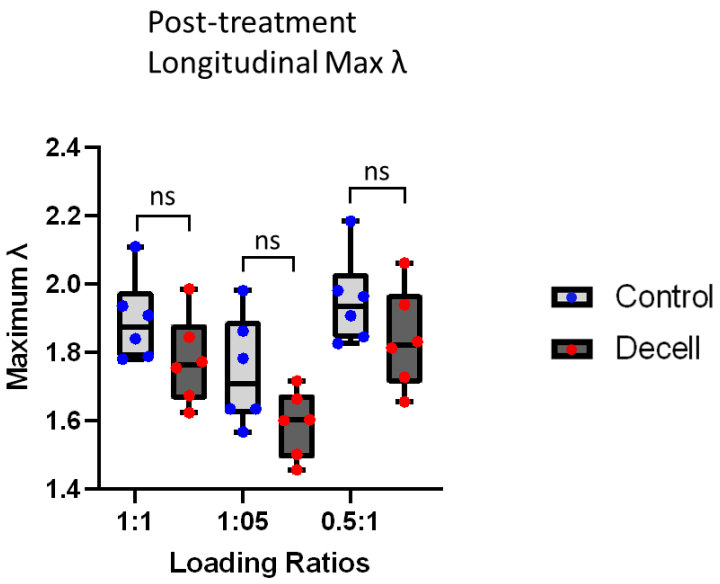

Figure 4-21: Post-treatment longitudinal maximum λ for control and decellularized tissues at different loading ratios are compared with an unpaired *t*-test. Statistical significance is indicated with * = $p < 0.05$, ** = $p < 0.005$, and ns = not statistically significant ($p \geq 0.05$).

The circumferential and longitudinal maximum λ values for the control and decellularized tissues were recorded, and the mean values were calculated. The percent change was calculated between the pre-treatment and post-treatment values. This is shown in **Tables 4-13** through **4-15**.

Table 4-13: Circumferential maximum λ values for control tissues.

Circumferential Max Stretch Control								
	Tissue 1	**Tissue 2**	**Tissue 3**	**Tissue 4**	**Tissue 5**	**Tissue 6**	**Mean ± SD**	**% Change**
1:1 Pre-treatment	1.634	1.761	1.776	1.800	1.714	1.804	1.748±0.065	11.17%
1:1 Post-treatment	1.947	1.925	1.894	2.025	1.824	2.045	1.943±0.083	
1:0.5 Pre-treatment	1.677	1.794	1.834	1.864	1.758	1.850	1.796±0.070	11.70%
1:0.5 Post-treatment	1.988	1.960	1.972	2.141	1.871	2.104	2.006±0.100	
0.5:1 Pre-treatment	1.562	1.669	1.695	1.696	1.644	1.657	1.654±0.049	8.28%
0.5:1 Post-treatment	1.867	1.732	1.742	1.856	1.715	1.832	1.791±0.068	

Table 4-14: Circumferential maximum λ values for decellularized tissues.

Circumferential Max Stretch Decell								
	Tissue 1	**Tissue 2**	**Tissue 3**	**Tissue 4**	**Tissue 5**	**Tissue 6**	**Mean ± SD**	**% Change**
1:1 Pre-treatment	1.645	1.581	1.767	1.830	1.714	1.825	1.727±0.100	9.27%
1:1 Post-treatment	1.773	1.840	1.893	2.107	1.787	1.921	1.887±0.122	
1:0.5 Pre-treatment	1.678	1.639	1.831	1.922	1.788	1.861	1.787±0.109	9.88%
1:0.5 Post-treatment	1.820	1.901	1.977	2.230	1.860	1.991	1.963±0.146	
0.5:1 Pre-treatment	1.564	1.465	1.625	1.718	1.568	1.661	1.600±0.088	6.70%
0.5:1 Post-treatment	1.688	1.631	1.712	1.933	1.593	1.688	1.708±0.119	

Table 4-15: Longitudinal maximum λ values for control tissues.

Longitudinal Max Stretch Control								
	Tissue 1	**Tissue 2**	**Tissue 3**	**Tissue 4**	**Tissue 5**	**Tissue 6**	**Mean ± SD**	**% Change**
1:1 Pre-treatment	1.563	1.634	1.573	1.558	1.551	1.615	1.582±0.034	19.63%
1:1 Post-treatment	1.935	1.908	1.788	1.839	1.780	2.108	1.893±0.123	
1:0.5 Pre-treatment	1.441	1.532	1.436	1.349	1.424	1.520	1.450±0.067	20.24%
1:0.5 Post-treatment	1.862	1.782	1.635	1.567	1.635	1.981	1.744±0.159	
0.5:1 Pre-treatment	1.606	1.665	1.601	1.608	1.581	1.651	1.619±0.032	20.54%
0.5:1 Post-treatment	1.981	1.963	1.846	1.907	1.825	2.184	1.951±0.130	

Table 4-16: Longitudinal maximum λ values for decellularized tissues.

Longitudinal Max Stretch Decell								
	Tissue 1	Tissue 2	Tissue 3	Tissue 4	Tissue 5	Tissue 6	Mean ± SD	% Change
1:1 Pre-treatment	1.510	1.465	1.593	1.660	1.589	1.610	1.571±0.071	13.01%
1:1 Post-treatment	1.623	1.845	1.772	1.985	1.674	1.755	1.776±0.129	
1:0.5 Pre-treatment	1.413	1.322	1.475	1.459	1.430	1.506	1.434±0.064	10.87%
1:0.5 Post-treatment	1.456	1.716	1.603	1.664	1.501	1.601	1.590±0.098	
0.5:1 Pre-treatment	1.542	1.514	1.632	1.721	1.637	1.645	1.615±0.076	13.80%
0.5:1 Post-treatment	1.656	1.939	1.831	2.061	1.727	1.813	1.838±0.146	

Thickness measurements were taken before and after treatment for both the control and decellularized groups and were compared using a paired *t*-test. For both groups, a statistically significant increase in thickness was observed following treatment. This is shown in **Figure 4-22**.

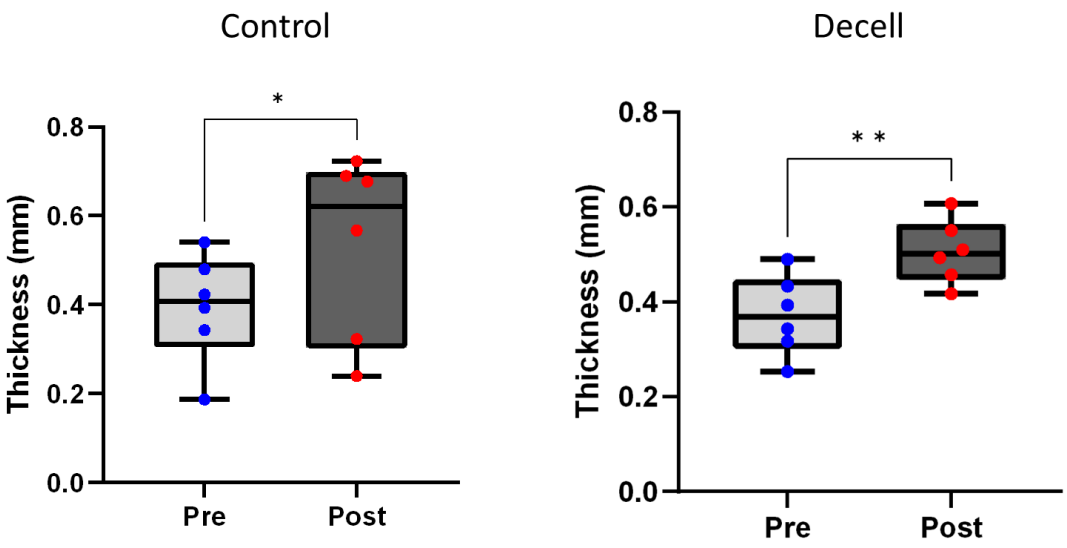

Figure 4-22: Thickness (mm) pre and post-treatment for control (left) and decellularized tissue (right). Pre-treatment values are compared to post-treatment values with a paired *t*-test. Statistical significance is indicated with * = $p < 0.05$, ** = $p < 0.005$, and ns = not statistically significant ($p \geq 0.05$).

Post-treatment thickness values for the control and decellularized groups were compared using an unpaired *t*-test. There were no statistically significant differences observed between the post-treatment thickness values. This is shown in **Figure 4-23**.

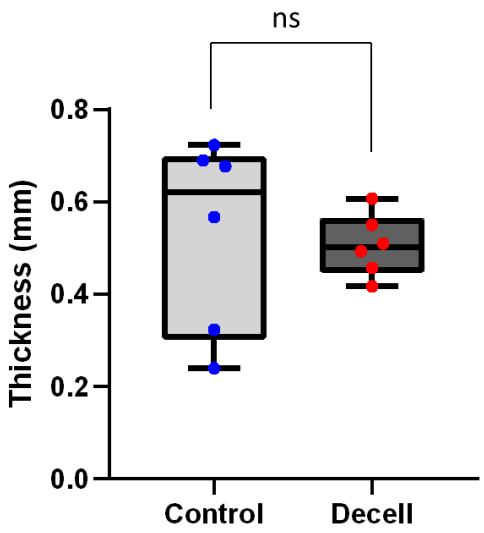

Figure 4-23: Post-treatment thickness (mm) for control and decellularized tissue are compared with an unpaired *t*-test. Statistical significance is indicated with * = $p < 0.05$, ** = $p < 0.005$, and ns = not statistically significant ($p \geq 0.05$).

The thickness values for the control and decellularized tissues were recorded, and the mean values were calculated. The percent change was calculated between the pre-treatment and post-treatment values. This is shown in **Table 4-17**.

Table 4-17: Thickness (mm) values for control and decellularized tissues

Tissue Thickness								
	Tissue 1	Tissue 2	Tissue 3	Tissue 4	Tissue 5	Tissue 6	Mean ± SD	% Change
Decell: Pre-treatment	0.343	0.253	0.490	0.317	0.433	0.393	0.372±0.085	36.02%
Decell: Post-treatment	0.493	0.417	0.510	0.457	0.550	0.607	0.506±0.067	
Control: Pre-treatment	0.187	0.540	0.423	0.393	0.480	0.343	0.394±0.123	36.06%
Control: Post-treatment	0.240	0.677	0.567	0.690	0.723	0.323	0.537±0.206	

For the following loading ratios (P_{CC}: P_{LL} = 1:1, 1:0.5, and 0.5:1) as well as the mounting position, the pre-treatment and post-treatment DOA was compared for the control and decellularized tissues. A paired *t*-test was performed between the pre-treatment and post-treatment values. There was no statistical significance found between the pre-treatment and post-treatment values for either the control group or the decellularized group. This is shown in **Figure 4-24**.

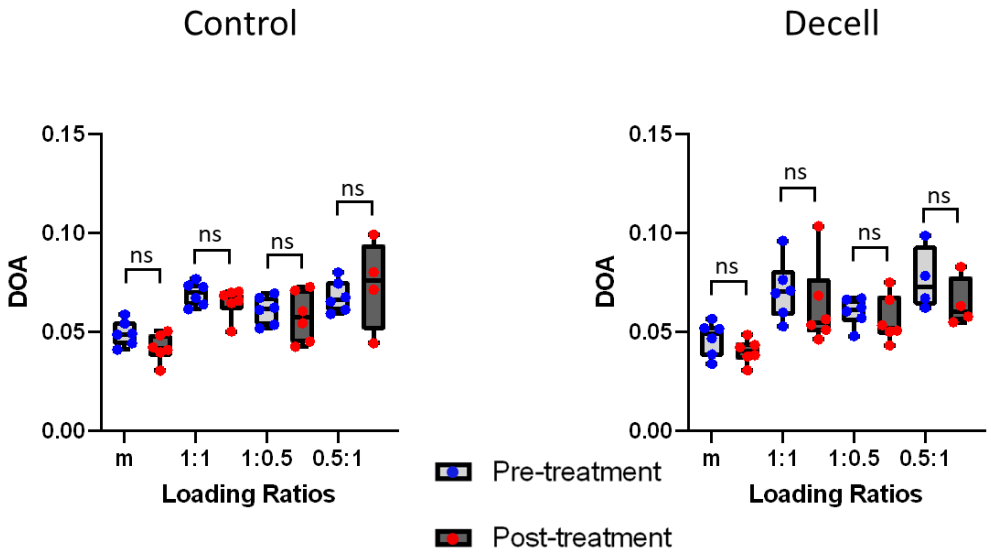

Figure 4-24: DOA for pre- and post-treatment for control (left) and decellularized tissue (right) at different loading ratios. Pre-treatment values are compared to post-treatment values with a paired *t*-test. Statistical significance is indicated with * = $p < 0.05$, ** = $p < 0.005$, and ns = not statistically significant ($p \geq 0.05$).

For the following loading ratios (P_{CC}: P_{LL} = 1:1, 1:0.5, and 0.5:1) as well as the mounting position, the post-treatment DOA was compared for the control and decellularized tissues using an unpaired *t*-test. There was no statistical significance found between the control group or the decellularized group. This is shown in **Figure 4-25**.

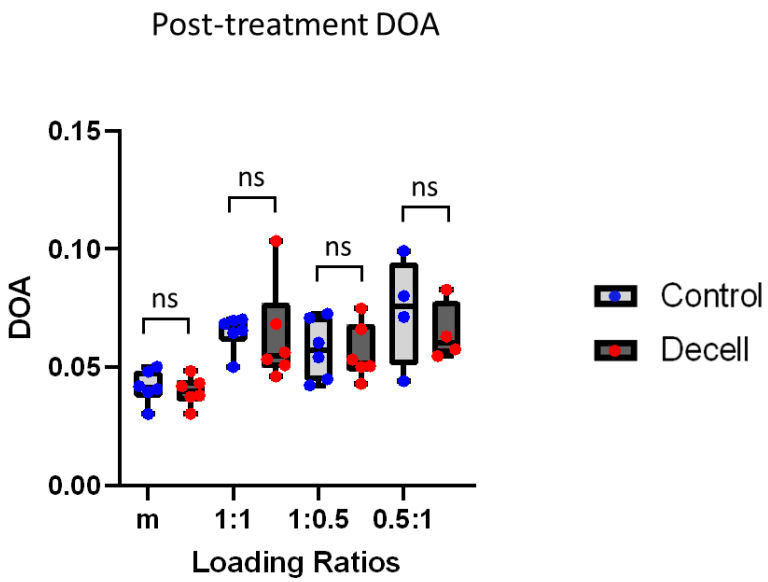

Figure 4-25: Post-treatment DOA for control and decellularized tissue at different loading ratios. Post-treatment values were compared with an unpaired *t*-test. Statistical significance is indicated with * = $p < 0.05$, ** = $p < 0.005$, and ns = not statistically significant ($p \geq 0.05$).

The DOA values for the control and decellularized tissues were recorded, and the mean values were calculated. The percent change was calculated between the pre-treatment and post-treatment values. Due to an error in the data procurement, some of the values are missing from the following tables. These missing values are marked "NA." This is shown in **Table 4-18** and **Table 4-19.**

Table 4-18: DOA for control tissues

DOA Control								
	Tissue 1	**Tissue 2**	**Tissue 3**	**Tissue 4**	**Tissue 5**	**Tissue 6**	**Mean ± SD**	**% Change**
m: Pre-treatment	0.0587	0.0491	0.0442	0.0409	0.0540	0.0485	0.0492±0.0065	-14.96%
m: Post-treatment	0.0421	0.0396	0.0482	0.0408	0.0503	0.0303	0.0419±0.0071	
1:1 Pre-treatment	0.0614	0.0672	0.0735	0.0727	0.0767	0.0638	0.0692±0.006	-6.29%
1:1 Post-treatment	0.0501	0.0656	0.0684	0.0704	0.0646	0.0698	0.0648±0.0075	
1:0.5 Pre-treatment	0.0536	0.0694	0.0610	0.0517	0.0671	0.0621	0.0608±0.0071	-5.23%
1:0.5 Post-treatment	0.0425	0.0710	0.0543	0.0451	0.0605	0.0727	0.0577±0.0127	
0.5:1 Pre-treatment	0.0675	0.0744	0.0590	0.0611	0.0800	0.0652	0.0679±0.008	8.62%
0.5:1 Post-treatment	0.0442	NA	0.0802	0.0991	0.0713	NA	0.0737±0.0228	

Table 4-19: DOA for decellularized tissues

DOA Decell								
	Tissue 1	**Tissue 2**	**Tissue 3**	**Tissue 4**	**Tissue 5**	**Tissue 6**	**Mean ± SD**	**% Change**
m: Pre-treatment	0.0386	0.0518	0.0467	0.0566	0.0337	0.0514	0.0465±0.0087	-13.91%
m: Post-treatment	0.0304	0.0485	0.0376	0.0420	0.0382	0.0433	0.0400±0.0061	
1:1 Pre-treatment	0.0596	0.0763	0.0708	0.0961	0.0526	0.0695	0.0708±0.0150	-10.94%
1:1 Post-treatment	0.0509	0.0534	0.0563	0.1035	0.0461	0.0683	0.0631±0.0212	
1:0.5 Pre-treatment	0.0569	0.0663	0.0603	0.0669	0.0478	0.0621	0.0601±0.0071	-6.12%
1:0.5 Post-treatment	0.0502	0.0506	0.0533	0.0750	0.0431	0.0662	0.0564±0.0118	
0.5:1 Pre-treatment	0.0622	NA	0.0783	0.0987	0.0670	NA	0.0765±0.0162	-15.59%
0.5:1 Post-treatment	0.0577	0.0548	0.0630	NA	NA	0.0828	0.0646±0.0126	

For the following loading ratios (P_{CC}: P_{LL} = 1:1, 1:0.5, and 0.5:1) as well as the mounting position, the pre-treatment and post-treatment θ_{fiber} was compared for the control and decellularized tissues. A paired *t*-test was performed between the pre-treatment and post-treatment values. There was high variance in both the control and decellularized tissue datasets, in part due to tissue heterogeneity. There was a statistically significant difference between the pre-treatment and post-treatment values for the θ_{fiber} values for the mounting position for both the control group and the decellularized group, however, none of the other loading ratios showed significantly altered θ_{fiber} values, as shown in **Figure 4-26**.

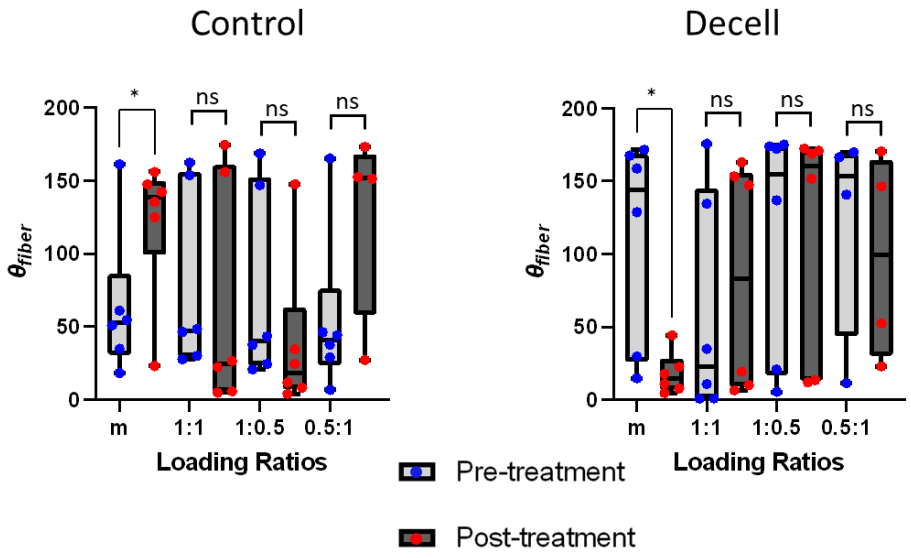

Figure 4-26: θ_{fiber} for pre- and post-treatment for control (left) and decellularized tissue (right) at different loading ratios. Pre-treatment values are compared to post-treatment values with a paired *t*-test. Statistical significance is indicated with * = $p < 0.05$, ** = $p < 0.005$, and ns = not statistically significant ($p \geq 0.05$).

For the following loading ratios (P_{CC}: P_{LL} = 1:1, 1:0.5, and 0.5:1) as well as the mounting position, the post-treatment θ_{fiber} was compared for the control and decellularized tissues using an unpaired *t*-test. There was a statistically significant difference between the control and decellularized post-treatment θ_{fiber} values in the mounting position, however, none of the other loading ratios exhibited significantly altered θ_{fiber} values. This is shown in **Figure 4-27**.

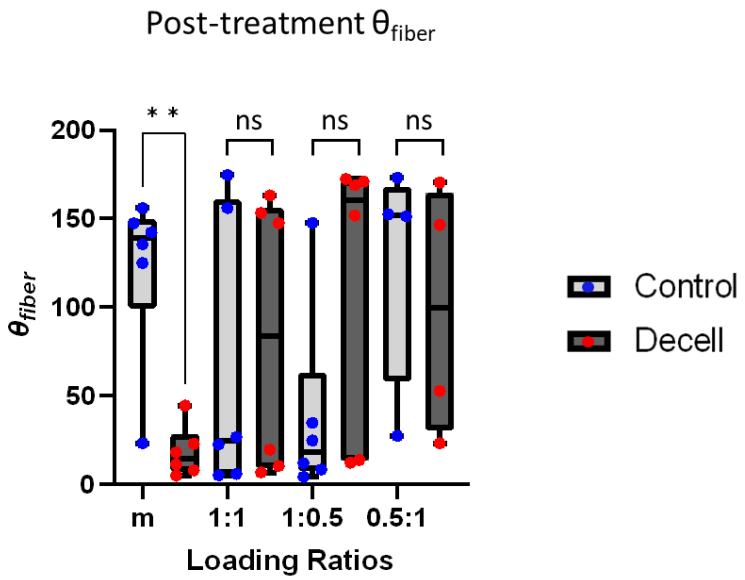

Figure 4-27: Post-treatment θ_{fiber} for control and decellularized tissue at different loading ratios. Post-treatment values were compared with an unpaired *t*-test. Statistical significance is indicated with * = $p < 0.05$, ** = $p < 0.005$, and ns = not statistically significant ($p \geq 0.05$).

The θ_{fiber} values for the control and decellularized tissues were recorded, and the mean values were calculated. The percent change was calculated between the pre-treatment and post-treatment values. Due to an error in the data procurement, some of the values are missing from the following tables. These missing values are marked "NA." This is shown in **Table 4-20** and **Table 4-21.**

Table 4-20: θ_{fiber} for control tissues

Fiber θ Control								
	Tissue 1	**Tissue 2**	**Tissue 3**	**Tissue 4**	**Tissue 5**	**Tissue 6**	**Mean ± SD**	**% Change**
m: Pre-treatment	50.92	61.10	18.29	161.07	54.52	34.94	63.47±50.25	91.43%
m: Post-treatment	135.47	142.27	23.06	147.47	124.85	155.91	121.51±49.37	
1:1 Pre-treatment	48.45	30.06	27.71	153.80	46.40	162.17	78.10±62.50	-16.76%
1:1 Post-treatment	4.98	26.61	5.71	155.85	174.57	22.34	65.01±78.32	
1:0.5 Pre-treatment	43.39	24.62	20.77	146.86	37.61	168.58	73.64±66.01	-47.76%
1:0.5 Post-treatment	11.71	34.64	4.13	147.50	8.30	24.53	38.47±54.59	
0.5:1 Pre-treatment	46.22	44.33	6.77	165.20	37.56	29.16	54.87±55.91	129.62%
0.5:1 Post-treatment	173.02	NA	27.28	152.47	151.24	NA	126.00±66.57	

Table 4-21: θ_{fiber} for control tissues

Fiber θ Decell								
	Tissue 1	**Tissue 2**	**Tissue 3**	**Tissue 4**	**Tissue 5**	**Tissue 6**	**Mean ± SD**	**% Change**
m: Pre-treatment	158.83	29.91	171.62	128.81	14.91	167.52	111.93±71.1	-83.83%
m: Post-treatment	17.97	7.67	4.71	11.05	22.83	44.37	18.10±14.49	
1:1 Pre-treatment	175.73	35.04	1.11	134.53	10.91	0.95	59.71±76.07	39.55%
1:1 Post-treatment	163.12	153.22	6.60	10.24	147.36	19.45	83.33±78.31	
1:0.5 Pre-treatment	5.67	20.95	173.85	136.87	172.25	175.04	114.1±79.52	0.73%
1:0.5 Post-treatment	151.73	170.89	168.93	172.36	12.08	13.64	114.94±79.42	
0.5:1 Pre-treatment	169.94	NA	166.44	140.69	11.50	NA	122.14±74.90	-19.67%
0.5:1 Post-treatment	170.37	146.40	23.12	NA	NA	52.61	98.12±71.29	

Color maps were generated for the LADA before and after treatment at four loading ratios (mounting, P_{CC}: P_{LL} = 1:1, 1:0.5, and 0.5:1). The colors correspond with the DOA of the tissue. The warmer colors represent higher DOA values, which indicate better collagen alignment. The cooler colors represent lower DOA values, which indicate more random fiber networks. Additionally, the orientation of the collagen fibers can be visualized by the white dashed lines, as shown in **Figure 4-28** and **Figure 4-29,** for pre- and post-treatment, between the control and decellularized groups, respectively.

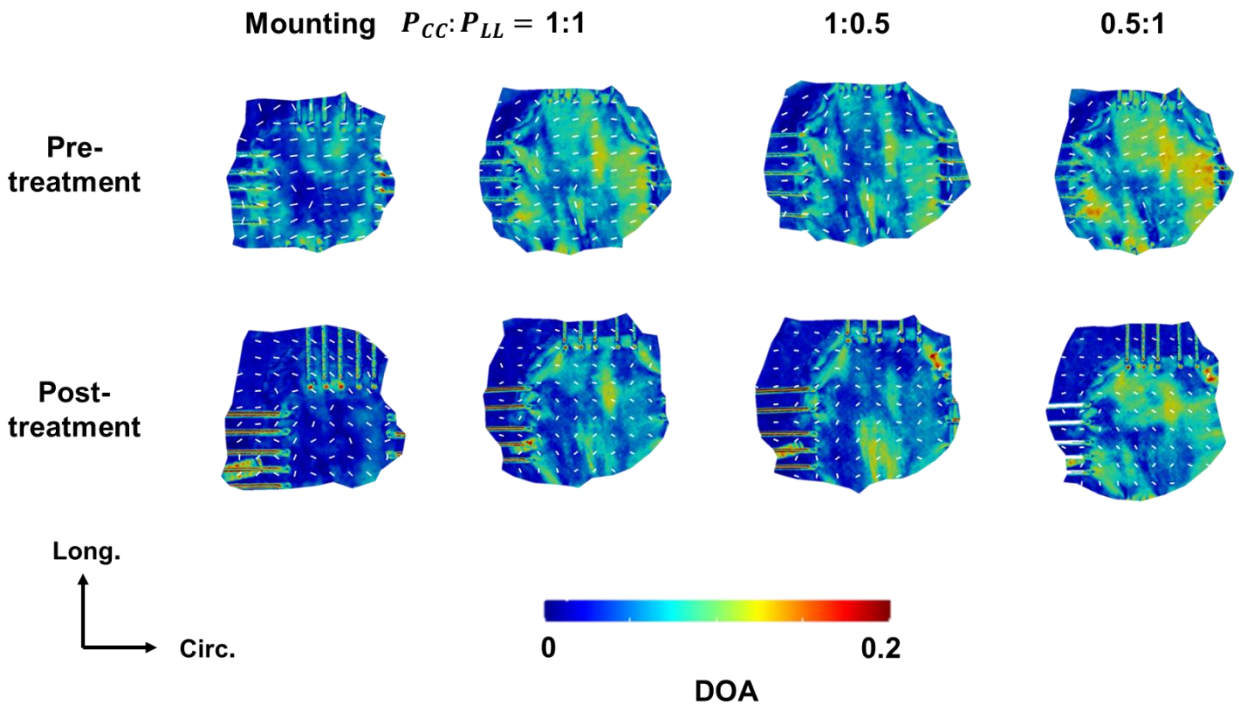

Figure 4-28: Color map of control LADA before and after treatment at different loading ratios. The colors correspond with the DOA and the white dashed lines correspond with the average θ_{fiber}.

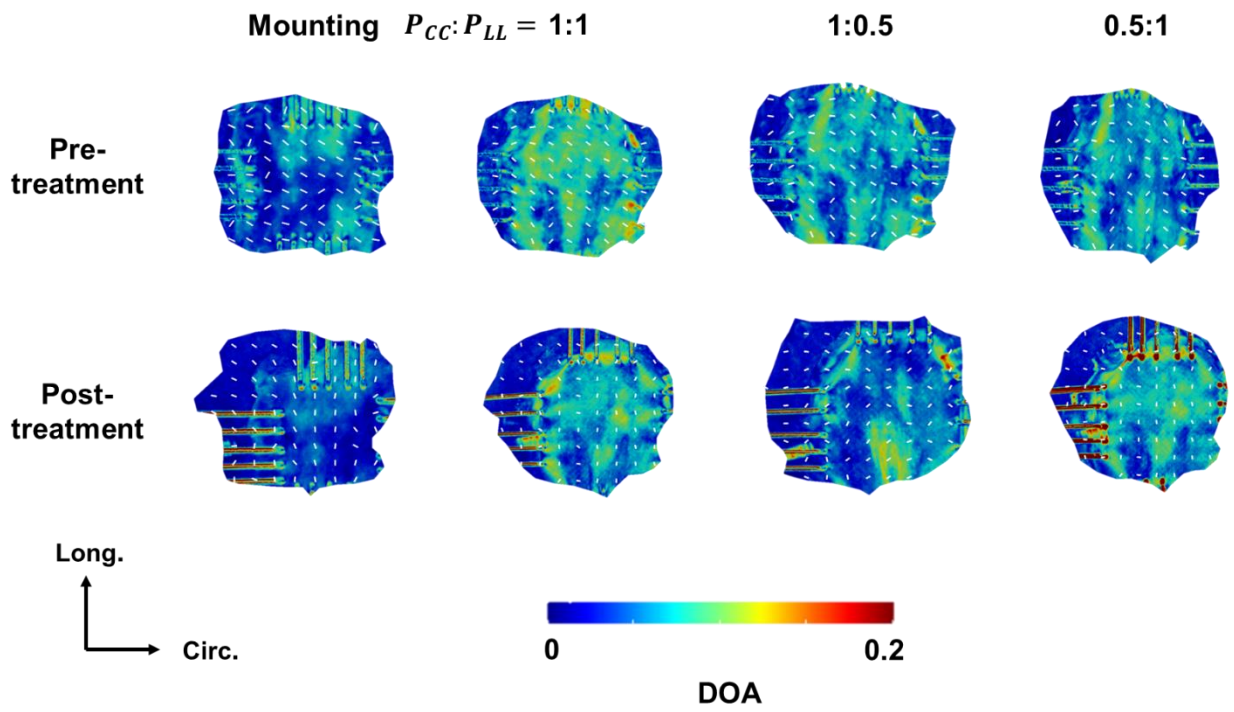

Figure 4-29: Color map of decellularized LADA before and after treatment at different loading ratios. The colors correspond with the DOA and the white dashed lines correspond with the average θ_{fiber}.

4.3 Discussion

For most tested parameters, there was a statistically significant difference between the pre- and post-treatment values. However, this difference was seen for both the control and decellularized groups. These changes in pre- and post-treatment values can be attributed to several things. First, soaking tissue samples in DI water can induce osmotic-related swelling, which can be seen by the increase in thickness post-treatment. This expansion can alter responses to mechanical stimuli[32]. Second, the effective testing region of the post-treatment samples were smaller than the pre-treatment samples. This was done to avoid the puncture marks made in the first iteration of biaxial testing. This change in testing region reduced the targeted force.

Furthermore, when the control and decellularized post-treatment specimens were compared using an unpaired *t*-test, there was no significant differences in all of the parameters except longitudinal E^{HT} in the P_{CC}: P_{LL} = 1:0.5 ratio and longitudinal λ^* in the P_{CC}: P_{LL} = 1:0.5 ratio. There was no significant difference between the control and decellularized post-treatment low-tension modulus in either direction. Furthermore, there was no significant difference in the high-tension modulus in the circumferential direction. Additionally, there was no significant difference between the post-treatment maximum λ in either direction, nor was there a significant difference between the post-treatment circumferential tissue extensibility values. This indicates that the decellularization procedure did not significantly alter the mechanical properties of the artery tissue.

To examine whether the decellularization procedure altered the collagen fiber orientation in the LADA tissue, polarized spatial frequency domain imaging (pSFDI) was performed. Generally, it was observed that when a biaxial load was applied and the tissue was stretched, the DOA increased. This was seen for both the control and decellularized specimens. This finding is supported by previous literature, and it is indicative of collagen fiber uncrimping and fiber realignment[7,30]. This collagen fiber uncrimping induces a strain-stiffening response and is an essential process in regulating arterial mechanical responses[33]. The results of the pSFDI experiments revealed that DOA was not significantly altered following treatment for either the control or decellularization groups. Furthermore, when the post-treatment DOA values were compared between the control and decellularized tissues, there was no significant difference. This demonstrates that the decellularization procedure did not significantly alter the DOA or collagen fiber uncrimping process.

Another parameter that was examined using pSFDI was the collagen fiber angle (θ_{fiber}). This parameter was highly varied between the tissue specimens. This variance in fiber orientation is seen in previous literature, in part due to tissue heterogeneity[7,30]. Furthermore, because this method is reliant on optical information pulled from imaged specimens, it is susceptible to mispredictions caused by folds in the tissue, impurities in the PBS bath, glare, and the formation of bubbles. This study revealed that the average θ_{fiber} was not significantly altered between following treatment in either of the control or decellularization groups in all loading ratios, except for the mounting position. Similarly, when comparing the post-treatment θ_{fiber} values between the control and decellularized tissues, only the mounting position showed any statistically significant difference. This suggests that when a physiologically relevant load is applied to the LADA tissue, the θ_{fiber} is not significantly altered following decellularization.

CHAPTER 5 – CONCLUSION AND FUTURE WORK

5.1 Conclusions

The results in this thesis provide valuable insight into how the chosen decellularization method impacts the mechanical and microstructural properties of porcine LADA tissue, as well as provides a template for how to analyze the impact of decellularization on soft tissue in general. The optimized decellularization procedure chosen for this thesis involves the LADA tissue being submerged in 0.5% Triton X-100 solution for 24 hours, followed by a rinse in DI water for 24 hours. Next, the tissue is submerged in an enzymic solution of 0.02 mg/mL of RNase and 0.2 mg/mL of DNase for 24 hours, followed by a rinse in PBS for 24 hours. When the tissue was analyzed using H&E stains, this decellularization procedure appeared to completely remove cellular components. This removal of cells is essential in the fabrication of TEVGs from native tissue in order to minimize host immune response. Further histological analysis using Masson's Trichrome and EVG revealed no major differences in the collagen and elastin components in the arteries following decellularization compared to the control. This suggests that the chosen decellularization method sufficiently removes cellular components from the arteries without damaging the extracellular matrix.

After determining that the chosen decellularization protocol effectively removed cellular components, biaxial mechanical testing and pSFDI were then performed to analyze the effect of decellularization on the LADA mechanical properties and collagen fiber architecture. The parameters that were evaluated included low tension elastic modulus (E^{LT}), high tension elastic modulus (E^{HT}), tissue extensibility (λ^*), and max stretch (λ) for the circumferential and longitudinal directions, as well as degree of anisotropy (DOA) and collagen fiber angle (θ_{fiber}). For the different loading ratios (P_{CC}: P_{LL} = 1:1, 1:0.5, and 0.5:1), there was no statistically

significant differences between the control and decellularized post-treatments E^{LT} or max stretch in either the circumferential or the longitudinal directions. For λ^*, there was a statistically significant difference in the $P_{CC}: P_{LL} =$ 1:0.5 ratio in the longitudinal direction, but there was no difference in any of the loading ratios in the circumferential direction. Similarly, for E^{HT}, there was a statistically significant difference in the $P_{CC}: P_{LL} =$ 1:0.5 ratio in the longitudinal direction, but there was no difference in any of the loading ratios in the circumferential direction. Furthermore, pSFDI analysis revealed that there was no statistically significant difference in the post-treatment DOA between the control and decellularized groups. Regarding θ_{fiber}, the only difference found between the control and decellularized group was in the mounting configuration. The post-treatment θ_{fiber} was not significantly different between the control and decellularized groups for the $P_{CC}: P_{LL} =$ 1:1, 1:0.5, and 0.5:1 ratios. These results indicate that the decellularization procedure did not drastically alter the mechanical properties or collagen fiber architecture. The preservation of mechanical properties and collagen fiber architecture is important to withstand the pressures of the host environment and to encourage cell growth and signaling.

5.2 Future Work

Recommendations for future work include the evaluation of the other extracellular matrix components, such as GAGs and proteoglycans. Additionally, decellularization studies should be expanded to the other regions of the LADA: the medial and distal regions. From there, whole vessel decellularization could be performed. Additional considerations for whole vessel decellularization include perfusion through the vessel. As this thesis focuses on the decellularization of small and flattened sections of the artery, further research into flow conditions should be investigated for whole vessel decellularization. Additionally, to overcome

the limitations of pSFDI mispredictions, future recommended work should verify the collagen fiber orientation using multi-photon microscopy. Furthermore, biocompatibility tests should be completed to ensure that there is no residual DNA or immunogens and that the detergent and enzyme residues do not negatively impact cell viability. To quantify residual DNA and immunogens, such as leukocyte antigens, ultraviolet-visual spectrophotometry should be conducted. Additionally, a cell viability assay should be conducted, such as a live/dead assay using Calcian AM and propidium iodide. Other tests to demonstrate biocompatibility include hemocompatibity tests to quantify hemolysis and thrombogenicity. After determining that the decellularized scaffolds are biocompatible, further work should be done looking into the recellularization of these scaffolds to examine cell growth and migration. Biaxial mechanical testing and pSFDI should also be performed following recellularization to evaluate changes to the mechanical and microstructural properties.

While more work needs to be done, the results in this thesis provide evidence for a decellularized based engineered vascular graft that minimizes host immune response while maintaining native tissue architecture and mechanical properties.

APPENDIX A – NOMENCLATURE

Table A-1. Description of the abbreviations used throughout the thesis.

Category	Abbreviation	Description
Anatomy	LADA	Left anterior descending artery
	ECM	Extracellular matrix
	RCA	Right coronary artery
	LMCA	Left main coronary artery
	LCA	Left circumflex artery
	ITA	Internal thoracic artery
	RA	Radial artery
	GSV	Great saphenous vein
	circ	Circumferential direction
	long	Longitudinal direction
Microstructure	GAG	Glycosaminoglycan
Pathology	CAD	Coronary artery disease
	MI	Myocardial infarction
	LVD	Left ventricular dysfunction
	HF	Heart failure
Treatment	CABG	Coronary artery bypass grafting
	ACE	Angiotensin-converting enzyme
	PCI	Percutaneous coronary intervention
	TEVG	Tissue engineered vascular graft
Reagents	SDS	Sodium dodecyl sulfate
	SD	Sodium deoxycholate
	CHAPS	3-[(3-cholamidopropyl)dimethylammonio]-1-propanesulfonate
	EDTA	Ethylenediaminetetraacetic acid
	DI	Deionized
	PBS	Phosphate-buffered saline
Histology	H&E	Hematoxylin and Eosin
	EVG	Elastic Van Gieson
Mechanics	λ	Tissue stretch
	E^{LT}	Low-tension elastic modulus
	E^{HT}	High-tension elastic modulus
	λ^{*}	Tissue extensibility
	1st PK	First-Piola Kirchhoff stress
	T	Membrane tension
	P_{CC}	Membrane tension in the circumferential direction
	P_{LL}	Membrane tension in the longitudinal direction
Imaging	DOA	Degree of optical anisotropy
	pSFDI	Polarized spatial frequency domain imaging
	I	Intensity
Miscellaneous	ns	Not significant (statistics)

APPENDIX B – DETAILED DECELLULARIZATION PROCEDURE

Appendix B describes the chosen coronary artery decellularization procedure.

1. The first decellularization solution is aa detergent solution containing 0.5% Triton X-100 in DI water. To make 500 mL of this solution, 2.5 mL Triton X-100 was mixed with 497.5 mL of DI water. This was mixed thoroughly at room temperature. This solution was stored at room temperature.
2. The second decellularization is an enzymatic solution containing 0.2 mg/mL DNase and 0.02 mg/mL RNase in PBS. To make this solution, 20 mg of DNase and 2 mg of RNase was gently mixed into 100 mL PBS, with 50 mMol $MgCl_2$ at room temperature. This solution was stored in a freezer at -20 °C.
3. Following isolation of the proximal coronary artery, it is submerged in the detergent solution for 24 hours at room temperature.
4. Next, the artery is removed from the detergent solution and moved to DI water for 24 hours at room temperature.
5. Next, the artery is removed from the DI water and submerged in the enzymatic solution for 24 hours at room temperature.
6. Finally, the artery is removed from the enzymatic solution and is moved to PBS for 24 hours at room temperature. This process is shown in **Figure B-1**.

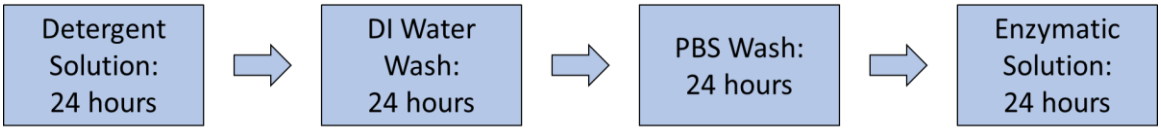

Figure B-1: Schematic showing the chosen decellularization procedure

APPENDIX C – DETAILED HISTOLOGY PROCEDURE

Appendix C describes the in-house histology preparation and H&E staining procedures. This procedure is modified from the Leica Biosystems procedures[34,35].

1. Following decellularization, the tissue samples were immediately placed into tissue cassettes and into a solution of 10% formalin for 48 hours and then subsequently stored in 20% ethanol at room temperature.
2. Using an automatic tissue processor (BioBase), the fixed samples in the tissue cassettes were dehydrated with alcohol, cleared with xylene, and infiltrated with wax. For proper infiltration, the wax was heated to 60°C. **Table C-1** shows the reagent concentration and exposure times.

Table C-1: Histology tissue processing exposure times

Reagent	Time (minutes)
70% Alcohol	30
95% Alcohol	30
100% Alcohol	30
100% Alcohol	30
100% Alcohol	30
100% Alcohol	60
Xylene	30
Xylene	15
Xylene	15
Wax	30
Wax	60

3. Next, the tissue samples were embedded in wax using a wax dispenser (BioBase). The samples were removed from the tissue cassettes and placed into metal paraffin molds. Heated

wax was poured into mold, and the tissue was oriented with the cross section facing down. This was done to view the artery layers. The bottom section of the tissue cassette was placed over the mold, and more wax was poured on. After an hour at room temperature, the wax was hardened enough to gently remove the embedded tissue and cassette from the mold.

4. Next, the tissue blocks were placed on a -23°C cooling plate for a few minutes. Using a microtome, 5-µm sections of the cooled tissue-containing paraffin blocks were cut. The tissue sections were placed in a 40°C water bath for a minute. Then, a charged microscope slide was submerged under the floating section and carefully lifted out of the water with the section. The slide then dried on a slide rack overnight.
5. Next, the slides underwent a deparaffinization process to remove the wax. The slides were submerged in xylene and alcohol, as outlined in **Table C-2**.

Table C-2: Deparaffinization exposure times

Reagent	**Time (minutes)**
Xylene	2
Xylene	2
100% Alcohol	2
100% Alcohol	2
100% Alcohol	2
95% Alcohol	2
Water	2

6. After deparaffinization, the slides underwent an H&E staining procedure. The reagents and exposure times are shown in **Table C-3**.

Table C-3: H&E staining procedure

Reagent	**Time (minutes)**
Hematoxylin	3
DI water	1
Acetic acid	1
DI water	1
Blueing	1
DI water	1
95% ethanol	30
Eosin Y	43 seconds
95% ethanol	1
100% ethanol	1
100% ethanol	1
Xylene	2
Xylene	2

7. After staining, the slides were dried for 5 minutes. Then, DPX mountant (Sigma-Aldrich) was used to apply coverslips. Slides were then imaged using a light microscope.

REFERENCES

1. Ogobuiro, I., Wehrle, C. J. & Tuma, F. Anatomy, Thorax, Heart Coronary Arteries. *StatPearls* (2022).
2. Chen, H. & Kassab, G. S. Microstructure-Based Biomechanics of Coronary Arteries in Health and Disease. *Journal of Biomechanics* **49**, 2548–2559 (2016).
3. Chen, H., Liu, Y., Slipchenko, M. N., Zhao, X., Cheng, J., & Kessab G. S. The Layered Structure of Coronary Adventitia under Mechanical Load. *Biophysical Journal* 101, 2555–2562 (2011).
4. del Monte-Nieto, G., Fischer, J. W., Gorski, D. J., Harvey, R. P. & Kovacic, J. C. Basic Biology of Extracellular Matrix in the Cardiovascular System, Part 1/4: JACC Focus Seminar. *Journal of the American College of Cardiology* **75**, 2169–2188 (2020).
5. Moore, K. H., Murphy, H. A. & George, E. M. The Glycocalyx: A Central Regulator of Vascular Function. *American Journal of Physiology-Regulatory, Integrative and Comparative Physiology* **320**, R508–R518 (2021).
6. Barallobre-Barreiro, J., Loeys, B., Mayr, M., Rienks, M., Verstraeten, A., &. Kovacic, J. C. Extracellular Matrix in Vascular Disease, Part 2/4: JACC Focus Seminar. *Journal of the American College of Cardiology* **75**, 2189-2203 (2020).
7. Pineda-Castillo, S. A., Aparico-Ruiz, S., Burns, M. W., Laurence, D. W., Bradshaw, E., Gu, T., Holzapfel, G. A. & Lee, C.-H. Linking the Region-Specific Tissue Microstructure to the Biaxial Mechanical Properties of the Porcine Left Anterior Descending Artery. *Acta Biomaterialia* **150**, 295–309 (2022).
8. Brown, J. C., Gerhardt, T. E. & Kwon, E. Risk Factors For Coronary Artery Disease. *StatPearls* (2022).

9. Klein, L. & Gheorghiade, M. Coronary Artery Disease and Prevention of Heart Failure. *Medical Clinics of North America* **88**, 1209–1235 (2004).
10. Wasilewski, J., Niedziela, J., Osadnik, T., Duszańska, A., Sraga, W., Desperak, P., Myga-Porosiło, J., Jackowska, Z., Nowakowski, A., & Głowacki, J. Predominant Location of Coronary Artery Atherosclerosis in the Left Anterior Descending Artery. The Impact of Septal Perforators and the Myocardial Bridging Effect. *Kardiochirurgia i Torakochirurgia Polska* **12**, 379-85 (2015).
11. Serruys, P. W., Kutryk, M. J. & Ong, A. T. DRUG THERAPY: Coronary-Artery Stents. *The New England Journal of Medicine* **354**, 483–495 (2006).
12. Banning, A. P. *et al.* Five-Year Outcomes After State-of-the-Art Percutaneous Coronary Revascularization in Patients with de Novo Three-Vessel Disease: Final Results of the SYNTAX II study. *European Heart Journal* **43**, 1307–1316 (2022).
13. Alexander, J. H. & Smith, P. K. Coronary-Artery Bypass Grafting. *The New England Journal of Medicine* **374**, 1954–1964 (2016).
14. Gaudino, M. *et al.* Mechanisms, Consequences, and Prevention of Coronary Graft Failure. *Circulation* **136**, 1749–1764 (2017).
15. Hall, A. B. & Brilakis, E. S. Saphenous vein graft failure: seeing the bigger picture. *Journal of Thoracic Disease* **1**, (2019).
16. Masroor, M., Zhou, K., Chen, C., Fu, X. & Zhao, Y. All we need to know about internal thoracic artery harvesting and preparation for myocardial revascularization: a systematic review. *Journal of Cardiothoracic Surgery* **16**, 354 (2021).
17. Pashneh-Tala, S., MacNeil, S. & Claeyssens, F. The Tissue-Engineered Vascular Graft—Past, Present, and Future. *Tissue Engineering Part B Review* **22**, 68–100 (2016).

18. Lee, H.-S., Heo, Y. J. & Chang, B.-C. Long-Term Digital Blood Flow After Radial Artery Harvesting for Coronary Artery Bypass Grafting. *European Journal of Cardio-Thoracic Surgery* **27**, 99–103 (2005).
19. Prim, D. A. *et al.* A Mechanical Argument for the Differential Performance of Coronary Artery Grafts. *Journal of the Mechanical Behavior of Biomedical Materials* **54**, 93–105 (2016).
20. Yaku, H. & Doi, K. Redo Coronary Artery Bypass Grafting. *General Thoracic Cardiovascular Surgery* **62**, 453–460 (2014).
21. Giannoukas, A. D. *et al.* Pre-Bypass Quality Assessment of the Long Saphenous Vein Wall with Ultrasound and Histology. *European Journal of Vascular and Endovascular Surgery* **14**, 37–40 (1997).
22. Niklason, L. E. & Lawson, J. H. Bioengineered Human Blood Vessels. *Science* **370**, eaaw8682 (2020).
23. Chang, W. G. & Niklason, L. E. A Short Discourse on Vascular Tissue Engineering. *Nature Partner Journals Regenerative Medicine* **2**, 1–8 (2017).
24. Wang, X., Chan, V. & Corridon, P. R. Decellularized Blood Vessel Development: Current State-of-the-Art and Future Directions. *Frontiers in Bioengineering Biotechnology* **10**, 951644 (2022).
25. Gilpin, A. & Yang, Y. Decellularization Strategies for Regenerative Medicine: From Processing Techniques to Applications. *Biomed Research International* **2017**, 9831534 (2017).
26. Funamoto, S. *et al.* The Use of High-Hydrostatic Pressure Treatment to Decellularize Blood Vessels. *Biomaterials* **31**, 3590–3595 (2010).

27. Grauss, R. W., Hazekamp, M. G., van Vliet, S., Gittenberger-de Groot, A. C., & DeRuiter, M. C. Decellularization of Rat Aortic Valve Allografts Reduces Leaflet Destruction and Extracellular Matrix Remodeling. *Journal of Thoracic Cardiovascular Surgery*. **126,** 2003-2010 (2003).
28. Schenke-Layland, K. *et al.* Impact of Decellularization of Xenogeneic Tissue on Extracellular Matrix Integrity for Tissue Engineering of Heart Valves. *Journal of Structural Biology* **143**, 201–208 (2003).
29. Lin, C.-H. *et al.* Decellularized Porcine Coronary Artery with Adipose Stem cells for Vascular Tissue Engineering. *Biomedical Materials* **14**, 045014 (2019).
30. Jett, S. V., Hudson, L. T., Baumwart, R., Bohnstedt, B. N., Mir, A., Burkhart, H. M., Holzapfel, G. A., Wu, Y. & Lee, C.-H. Integration of Polarized Spatial Frequency Domain Imaging (pSFDI) with a Biaxial Mechanical Testing System for Quantification of Load-Dependent Collagen Architecture in Soft Collagenous Tissues. Acta Biomaterialia 102, 149-168 (2020)
31. Cheng, S., Clarke, E. C. & Bilston, L. E. The Effects of Preconditioning Strain on Measured Tissue Properties. *Journal of Biomechanics* **42**, 1360–1362 (2009).
32. Salinas, S. D., Clark, M. M. & Amini, R. Mechanical Response Changes in Porcine Tricuspid Valve Anterior Leaflet Under Osmotic-Induced Swelling. *Bioengineering* **6**, 70 (2019).
33. Wang, R., Brewster, L. P. & Gleason, R. L. In-Situ Characterization of the Uncrimping Process of Arterial Collagen Fibers Using Two-Photon Confocal Microscopy and Digital Image Correlation. *Journal of Biomechanics* **46**, 2726–2729 (2013).

34. Tissue Processing Overview: Steps & Techniques for Histopathology. https://www.leicabiosystems.com/us/knowledge-pathway/an-introduction-to-specimen-processing/.
35. An Intro to H&E Staining: Protocol, Best Practices, Steps & More. https://www.leicabiosystems.com/us/knowledge-pathway/he-staining-overview-a-guide-to-best-practices/.